1965

Water vapor-sodium montmorillonite interaction

Gilbert Leroy Roderick
Iowa State University

66–3005

RODERICK, Gilbert Leroy, 1933–

WATER VAPOR–SODIUM MONTMORILLONITE INTERACTION.

Iowa State University of Science and Technology
Ph.D., 1965
Engineering, civil

University Microfilms, Inc., Ann Arbor, Michigan

WATER VAPOR-SODIUM MONTMORILLONITE INTERACTION

by

Gilbert Leroy Roderick

A Dissertation Submitted to the
Graduate Faculty in Partial Fulfillment of
The Requirements for the Degree of
DOCTOR OF PHILOSOPHY

Major Subject: Soil Engineering

Approved:

Signature was redacted for privacy.
In Charge of Major Work

Signature was redacted for privacy.
Head of Major Department

Signature was redacted for privacy.
Dean of Graduate College

Iowa State University
Of Science and Technology
Ames, Iowa

1965

TABLE OF CONTENTS

INTRODUCTION

Clay-water systems are of prime importance in engineering usage of soils, as for example in the prediction of bearing capacity, skin friction on piles, or settlement. Past research on these matters has emphasized mechanical aspects of soil-water systems. It has been recognized, however, that some problems such as secondary consolidation, swelling pressures, and cohesion (as applied in soil mechanics) are not solvable by a mechanistic approach. Therefore, it appears that a more fundamental knowledge of the clay-water system is essential for understanding and predicting the soil mechanics behavior of clays. We may note some interesting parallels in other fields, e.g. the role of dislocation theory in modern ceramics and metallurgy or the importance of bond energy concepts in materials science.

Sodium montmorillonite was chosen as the material for this investigation since the expansive clays are the most important in engineering practice. Also, this choice gives the opportunity to study the phenomenon of interlayer adsorption of water. The objectives of the investigation were to obtain successive complete adsorption-desorption isotherms for water vapor on sodium montmorillonite and X-ray diffraction data during adsorption and desorption, and to deduce from the data information for the interpretation of the various portions of the sorption isotherms, the manner in which water

enters between clay layers, external and internal surface areas, free energy changes on adsorption, expansion energies and swelling pressures.

THEORY AND REVIEW OF LITERATURE

Bangham (3,4) was first to show that the Gibbs adsorption equation could be used to determine the free surface energy changes that occur during adsorption of vapors on solid surfaces. Others have used Gibbsian methods to show that the free energy of immersion of a solid surface in saturated vapor can be calculated from vapor adsorption data (2,8,35). Jura and Harkins (39) showed that the formulae given, when expanded, are identical to that of Bangham. The equation for the free energy of immersion of a non-porous wettable surface in the saturated vapor, as given by Boyd and Livingston (8), can be made to read:

$$\Delta F = (\gamma_{sl} - \gamma_{so} + \gamma_{lv}) = -\frac{RT}{M\Sigma}\int_0^{p_o}\frac{q}{p}dp \qquad (1)$$

where γ_{sl} is the solid-liquid interfacial tension, γ_{so} the surface tension of the solid in vacuum, γ_{lv} the surface tension of the liquid in contact with its own vapor; q is the mass of vapor adsorbed by a unit mass of solid at pressure p; and R, T, M, Σ and p_o are the gas constant, absolute temperature, molecular weight of the vapor, specific surface of the solid and the saturation pressure, respectively. By substituting $p_o d(\frac{p}{p_o})$ for dp, Equation 1 can be changed to:

$$\Delta F = -\frac{RT}{M\Sigma}\int_0^1 \frac{q}{p/p_o}d(p/p_o) \qquad (2)$$

which is a more convenient form to use.

ΔF given by Equation 2 may be interpreted as the free energy change accompanying the process of transferring saturated vapor onto a unit area of solid surface; the process is terminated when the equilibrium pressure equals p_o. If the adsorbent is a mass of non-interacting fine powder wettable by the liquid, capillary condensation in the contact zones of the particles theoretically fills the voids with the liquid before the final saturation pressure is attained. In such cases therefore,

$$\Delta F = \gamma_{sl} - \gamma_{so} \qquad (3)$$

i.e., ΔF should be the free energy of immersion of a unit area of solid surface in the bulk liquid. Bartell and his co-workers (18,21,26) extended this view in the case of porous solids and compressed powders of non-porous solids; they have also shown that the validity of this point of view does not depend on the degree of compression of the powder (18). In spite of the fact that the solids used are wettable, some investigators (8,39) calculate ΔF by an extrapolation to saturation pressure and identify it with the free energy of immersion in saturated vapor, assuming that no capillary condensation takes place. To obtain the free energy of immersion in the bulk liquid they make a correction which amounts to subtracting the surface tension of the liquid from ΔF. The assumption of no capillary condensation, and the steepness of

the adsorption isotherm near the saturation pressure, introduce uncertainties in the free energy of immersion determined in this manner (18). For these reasons and because of the porous nature of clay minerals, a particular effort was made to actually reach saturation in the present study. The free energy of immersion in the bulk liquid was calculated directly from Equation 2 by graphical integration.

If the material being investigated consists of interacting solid particles, Hirst (33) and Demirel (20) independently have shown that Equation 3 must be modified by introducing a term representing the particle interaction. If the solid powder adsorbent has a rigid structure, ΔF as given by Equation 2 is equal to that expressed by Equation 3. When the adsorbate penetrates into interstices of interacting solid surfaces and causes a separation against the forces of interaction, Equation 3 may be modified as given by Demirel (20):

$$\Delta F = (\gamma_{sl} - \gamma_{so}) + \alpha\Delta V \qquad (3a)$$

where α is the interstitial surface area per cm^2 of total surface and ΔV is the free energy change per cm^2 of the interstitial surface due to separation of particles against the force of interaction (56, p. 253). Therefore, with clay minerals the free energy change given by Equation 2 is equivalent to that expressed by Equation 3a. The term $(\gamma_{sl}-\gamma_{so})$ will be called the free energy of immersion of the solid in the liquid and ΔF the free energy of wetting of the solid

by the liquid.

Brunauer et al. (13,16) developed their theory of multimolecular adsorption (BET theory) by a method which was a generalization of Langmuir's treatment of the unimolecular layer. Their basic assumption was that the forces chiefly responsible for the binding energy of multimolecular adsorption are the same as those responsible for condensation. For adsorption on a free surface they derived the equation:

$$v = \frac{v_m C p}{(p_o - p)[1 + (C - 1)p/p_o]} \tag{4}$$

which, for purposes of testing, can be put in the more convenient form:

$$\frac{p}{v(p_o - p)} = \frac{1}{v_m C} + \frac{C - 1}{v_m C}\frac{p}{p_o} \quad . \tag{4a}$$

In Equations 4 and 4a, v is the volume of vapor adsorbed at pressure p, v_m the volume of vapor adsorbed when the surface of the adsorbent is covered by a unimolecular layer of adsorbate and p_o the saturation pressure. The constant C is approximately given by the equation:

$$C = e^{(E_1 - E_L)/RT} \tag{5}$$

where E_1 is the heat of adsorption of the first layer and E_L is the heat of liquefaction. When the amount of vapor adsorbed is expressed in terms of mass, Equation 4a becomes:

$$\frac{p}{q(p_o - p)} = \frac{1}{q_m C} + \frac{C - 1}{q_m C} \frac{p}{p_o} \qquad (4b)$$

where q is the mass of vapor adsorbed at pressure p and q_m is the mass adsorbed at monolayer coverage of the adsorbent surface. Brunauer and his co-workers (13,15) developed a more general isotherm equation which considers factors limiting the number of layers that can be adsorbed and also includes capillary condensation. At low values of relative pressures their more general equation reduces to Equation 4a or 4b. Therefore, according to BET theory, physical adsorption in the low pressure range may be characterized by the two parameters q_m and C. Values of these parameters can be determined if a plot of $\frac{p}{q(p_o - p)}$ versus p/p_o from the experimental data gives a straight line as predicted by Equation 4b.

The parameter C includes the average heat of adsorption for the first layer, E_1. The values calculated by Equation 5 are less than measured heats of adsorption but are of the same order of magnitude (14). Clampitt and German (17) have shown that the heats of adsorption of thin films of liquid are different than that of the bulk liquid, and that they are calculable from the film thickness. They assumed that the heat of vaporization for second and higher layers is not a constant equal to the heat of vaporization of the bulk liquid as assumed in the BET theory, but that it varies depending on the film thickness. They re-derived the two parameter BET

equation; their treatment did not change its form but did change the meaning of C. In their treatment the exponential term in C is $E_1 - E_L + (\Delta H_s - E_L)$ rather than just $E_1 - E_L$. The correction term $(\Delta H_s - E_L)$, where ΔH_s is the heat of vaporization of the surface layer, accounts for the differences in the heat of vaporization of successive layers. By applying this correction they obtained much better agreement between $E_1 - E_L$ values determined from adsorption data and heat of emersion experiments (14). Clampitt and German's correction value for water is $(\Delta H_s - E_L) = -1700$ cal/mole. Goates and Hatch (28) also used a slightly different approach than that used by Brunauer et al. (16) and made a new development of their equation. The form of the equation remained the same but the constant C was shown to be given by:

$$C = e^{(\Delta F_1^\circ - \Delta F_L^\circ)/RT} \qquad (6)$$

where ΔF_1° is the standard Gibbs free energy of adsorption (standard adsorption potential) of the gas on the bare solid surface, and ΔF_L° is the standard Gibbs free energy of condensation of the adsorbate. As pointed out by Deitz (19), the study of multilayer adsorption has developed in several directions since the BET theory was proposed but--"Other than to demonstrate the great complexity of the problem, there has been no real breakthrough since the BET theory was formulated."

When the area, s, occupied by one molecule of the adsorbate on the solid surface is known, the specific surface,

Σ, of the solid can be calculated from the parameter q_m of the BET equation by:

$$\Sigma = \frac{Nq_m s}{M} \tag{7}$$

where N is Avogadro's constant, M is the molecular weight of the adsorbate and q_m is expressed for one gram of the adsorbent. Assuming closet packing, Brunauer (13, p. 287) gave the following expression for the area covered by a molecule of adsorbate:

$$s = (4)(0.866)\left(\frac{M}{N\delta\sqrt{2}}\right)^{2/3} = 1.091\left(\frac{M}{N\delta}\right)^{2/3} \tag{8}$$

where δ is the density of the solidified or liquefied adsorbate. The coefficient 1.091 is called the packing factor; its value for an adsorbate may vary from one adsorbent to another depending on the packing and on the variation of adsorbent pores (41). Equation 7 can be used to determine specific surface areas of adsorbents if the cross-sectional area of the adsorbate molecule is known; or it can be used to determine the area occupied by an adsorbate molecule if the specific surface is known. Using nitrogen as an adsorbate, Emmett et al. (22) obtained specific surface areas of soil colloids ranging from 41 to 71 m^2/gm. Brunauer (13, p. 357), using the water adsorption data of Hendricks et al. (32), obtained a specific surface of 400 m^2/gm for montmorillonite.

Zettlemoyer et al. (63) used ammonia adsorption on Wyoming bentonite and obtained a value of 556 m^2/gm; they obtained 34.5 m^2/gm with nitrogen as an adsorbate. Mooney et al. (51) used water desorption data to obtain values of about 800 m^2/gm (one layer of water between interlayer surfaces) for sodium and hydrogen montmorillonites but could not duplicate their results in a later study (52). Goates and Hatch (28) found a value of 303 m^2/gm with water adsorption on montmorillonite. Orchiston (55) obtained 336 m^2/gm with water vapor and sodium saturated montmorillonite. Johansen and Dunning (36), with sodium montmorillonite, got 38 m^2/gm with nitrogen, 203 m^2/gm with water vapor adsorption data and 250 m^2/gm with water vapor desorption data. All of the areas mentioned above were based on closest packing of the adsorbate on the clay surfaces. The large differences between values determined with nitrogen and those for ammonia and water vapor are attributed to the ability of the latter to penetrate between the montmorillonite layers while nitrogen covers only the external surfaces. The specific surfaces obtained from ammonia and water vapor sorption data, except for the one determination by Mooney et al. (51), were substantially less than that calculated from crystallographic data.

Other investigators (6,20,23,24,31,42) have postulated that water is adsorbed on the basal surfaces of clay minerals in certain spatial geometric arrangements which result in a looser packing of the water molecules. If the arrangement of

the molecules on the surface were known the area occupied per molecule could be calculated and used in Equation 7 to determine values for the specific surface.

Several investigators have studied the expansion of montmorillonites on adsorption of water between the clay layers. Nagelschmidt (53) showed that there was apparently a continuous variation of the basal spacings with water content. Bradley, Grim and Clark (9) found that the water molecules are adsorbed in monomolecular layers between the clay layers. From studies with oriented samples they found no evidence of a gradual swelling but rather a series of apparently definite and discrete hydrates. Hendricks et al. (32) reported the basal spacing varies continuously but not uniformly with water content; this results from an averaging effect from a lattice containing various numbers of water layers in different parts. Mering (47) found that the formation of discrete monomolecular layers of water does not hold precisely at low moisture contents when the adsorbed ion hydrates, e.g. Ca^{++} or Mg^{++}; for sodium montmorillonite hydration seemed to occur by complete molecular layers. Mooney et al. (52) used the data of Hendricks et al. (32) and their own to show a step-wise uptake of interlayer water with increasing humidity; however, they disregarded much of the data of Hendricks et al. Gillery (27) found that well defined hydrates exist over certain ranges of vapor pressure and that between these ranges mixed layers of the hydrates predominate. From the studies mentioned above,

and others (20,48), it has been quite well established that the separation of clay layers is due to the adsorption of integral molecular layers of water; the apparently continuous change in observed basal spacings results from random alternation of layers at various spacings. However, the relationship between relative humidities and layer separation is not well defined; the data reported for homoionic, e.g. sodium, montmorillonites show considerable variation (20,27,32,48,52).

MATERIALS

Sodium Montmorillonite

The sodium montmorillonite used was prepared for earlier investigations and the method of preparation has been described in detail elsewhere (20,58). A commercially available Wyoming bentonite, produced by the American Colloid Company and known by the trade name Volclay-SPV, was used. According to the producer it consists of 90 percent montmorillonite, essentially sodium montmorillonite, and 10 percent other minerals such as fedlspar, quartz and volcanic glass. The Volclay-SPV was freed from coarse grained impurities by a repeated (12 times) sedimentation process. An X-ray diffraction pattern from a dried sample of the suspension after the last sedimentation is shown in Figure 1.

Sodium montmorillonite was prepared from the purified bentonite by mixing a saturated sodium chloride solution with the suspension obtained from the sedimentation process. This mixture was stirred for 24 hours and the clay was then separated by means of a super-centrifuge. This process was repeated five times to assure replacement by sodium ions of all the cations associated with the montmorillonite. The free electrolyte was removed from the sample by dispersing in distilled water and centrifuging. This was repeated several times until the material was free of chloride ions. The physical and chemical properties were determined by standard

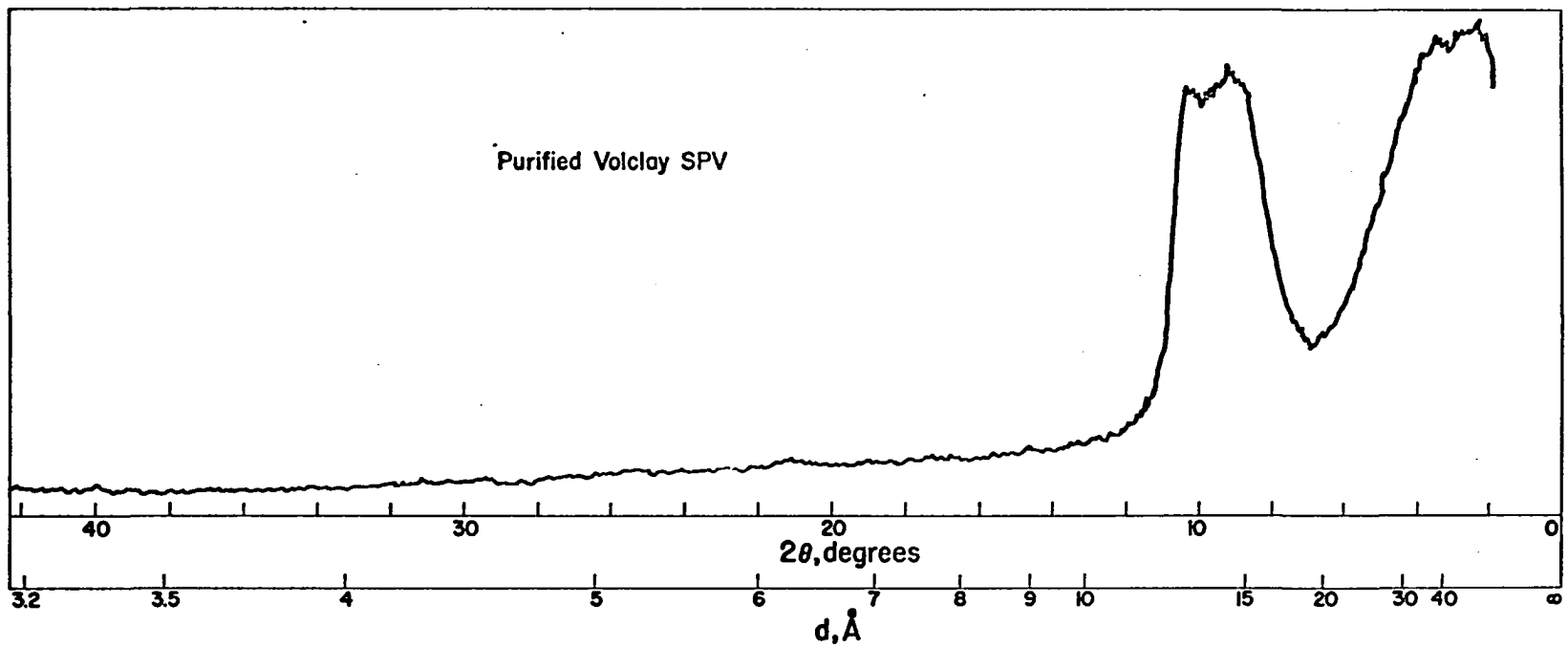

Figure 1. X-ray diffraction chart of purified Volclay-SPV obtained by using filtered chromium radiation

procedures and are presented in Table 1.

Table 1. Properties of the sodium montmorillonite

Physical properties	
Liquid limit, %[a]	968
Plastic limit, %[b]	51
Plasticity index, %	917
Shrinkage limit, %[c]	17
Centrifuge moisture equivalent, %[d]	882
Chemical properties	
Cation exchange capacity, m.e./100 gm[e]	94
pH[f]	7.55

[a]ASTM Method D423-54T.

[b]ASTM Method D424-54T.

[c]ASTM Method D427-61.

[d]ASTM Method D425-39.

[e]Ammonium acetate method.

[f]Glass electrode method using suspension of 1 gram of soil in 30 cc of distilled water.

Distilled Water

Distilled water used for preparation of the sample was obtained from a steam operated SLH-2 Barnstead still which produces, when fresh, practically carbon dioxide free water with a pH approaching 7. For the adsorption experiments this

distilled water was triple distilled just before introducing into the apparatus.

Sodium Chloride

Sodium chloride used in preparation of the sample was a reagent grade chemical meeting A.C.S. specifications.

Mercury

Mercury used in the diffusion pump and manometers was triple distilled C.P. grade.

METHODS OF INVESTIGATION

The adsorption isotherms were determined by the gravimetric method (13). The X-ray diffraction method (10) was used for studying the interlayer spacings at varying relative pressures of water vapor.

Adsorption Apparatus

The adsorption apparatus was constructed and used for earlier investigations (20,58). Some modifications were made in the permanent water reservoir set up and in the method of circulation of water in the thermostat. Also, a more sensitive spring balance was used.

The apparatus consisted of an adsorption chamber, with a McBain-Bakr (46) quartz spring balance, connected to a vacuum train by a large mercury-sealed stopcock and immersed in a water thermostat at 24.36°C. The vacuum train was a rotary single stage forepump (Cenco-Hyvac), a single stage mercury diffusion pump, a liquid nitrogen filled cold trap and a McLeod gauge. The plexiglass thermostat was fitted with optical glass observation windows for pressure and balance readings. It was equipped with a tap water cooling coil, a Beckman thermometer reading to 0.01° C, a continuous heater and an intermediate heater--mercury regulator--relay circuit. The Beckman thermometer was calibrated against a N.B.S. certified thermometer at the thermostat temperature. The heaters were two 100 watt light bulbs with variable transformer

voltage control. The water in the thermostat was kept in constant circulation by bubbling air into the tank near the bottom. Room temperature was maintained at about 3° C above the thermostat temperature.

Figure 2 is a schematic representation of the adsorption apparatus. Bulb "A" was the permanent water reservoir. "B" was a simple mercury manostat-manometer combination for transferring water vapor into the adsorption chamber "C" and for measuring vapor pressures. Mercury in "B" could be raised and lowered through air trap "D" by using a two-way mercury sealed stopcock "E" joining mercury reservoir "F" to a water aspirator. All glass parts were pyrex and high vacuum silicone grease was used at all joints. The quartz spring balance[1] "G" was suspended into the adsorption chamber from a hook attached to a mercury sealed ground glass stopper "H". Sample holder "I" was suspended from the hangdown loop of the spring balance. The sample holder was made from thin walled glass tubing and weighed less than 0.3 gram.

The load capacity of the balance was one gram and the balance extension at this load was 20 cm. From the manufacturer's data, the balance sensitivity was 0.210 mm/mg. Balance extensions were observed through the thermostat's optical glass window with an optical reader[1] which had a 5 mm objective field divided into 1000 divisions by a filar

---

[1]Obtained from Microchemical Specialties Co., Berkeley, California.

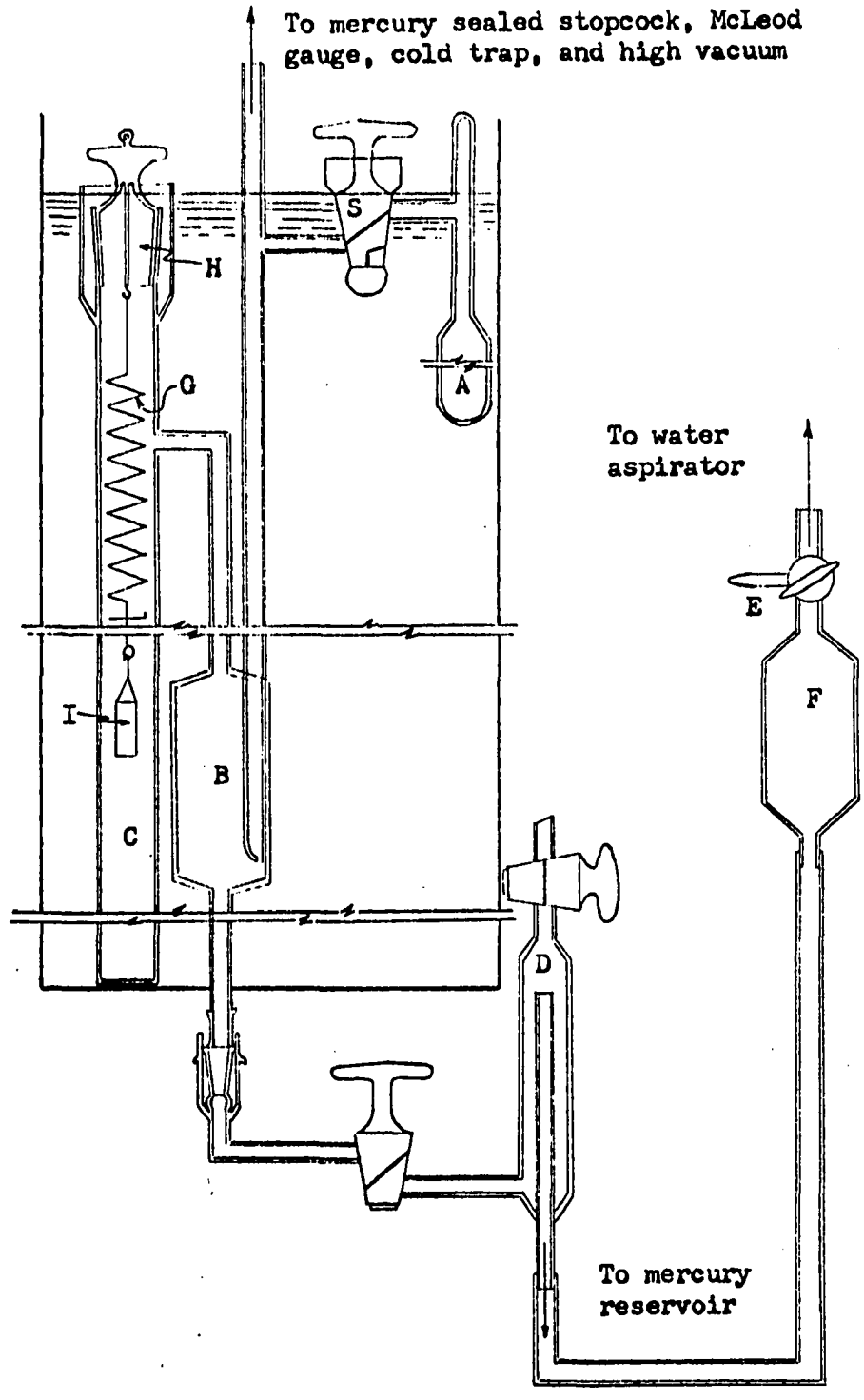

Figure 2. Schematic representation of the adsorption apparatus

micrometer eyepiece with a movable crossline. As certified by the manufacturer, 398.9 ± 0.1 divisions of the micrometer was equivalent to 2.0000 ± 0.00005 mm. The length of one division calculated from this information was 0.005013 ± 0.000002 mm (60). Therefore, the balance sensitivity was 0.0239 mg/division of the optical reader.

A cathetometer reading to 0.02 mm was used for measuring mercury levels in manometer "B" by observing through the optical glass window.

The adsorption apparatus, optical reader and cathetometer were securely mounted on a rigid steel frame tied to a heavy soapstone table top in order to prevent, as much as possible, differential movements. The apparatus is pictured in Figure 3.

Apparatus for X-ray Diffraction Study

The apparatus used in the X-ray study consisted of a Rigaku-Denki controlled atmosphere high temperature X-ray diffractometer attachment converted to serve as an adsorption chamber. The furnace and furnace support base were removed and a stainless steel sample holder, Figure 4, was constructed to take their place. This sample holder could be aligned by using the translation, rotation and inclination controls provided for alignment of the furnace. The arrangement of the water reservoir source for vapor, the manometer for pressure readings, the mercury sealed stopcock connection between the reservoir and adsorption chamber and the X-ray windows are

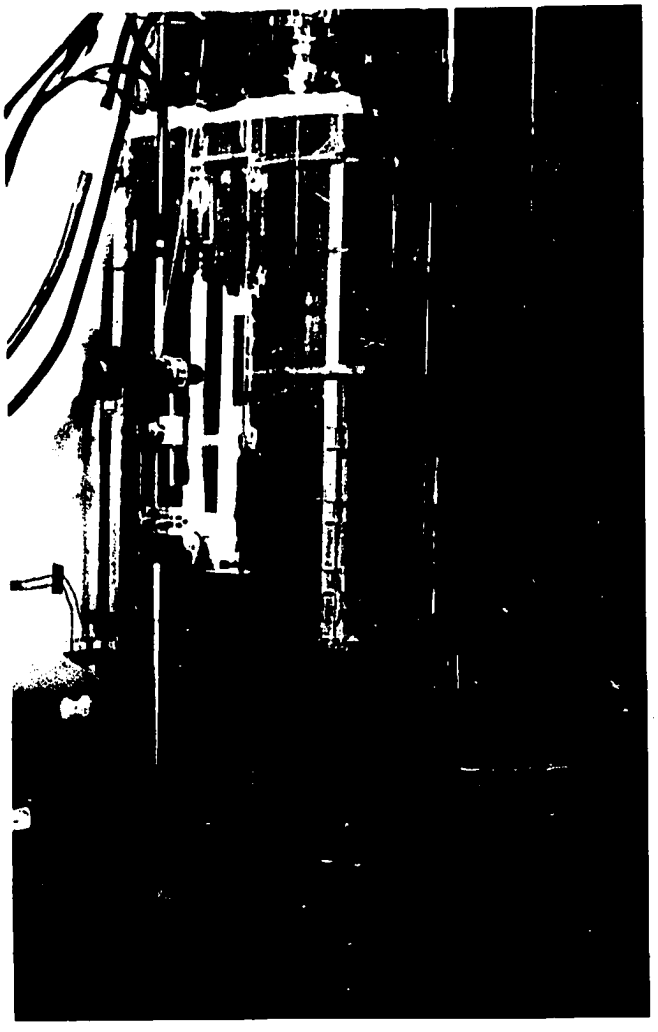

Figure 3. Adsorption apparatus

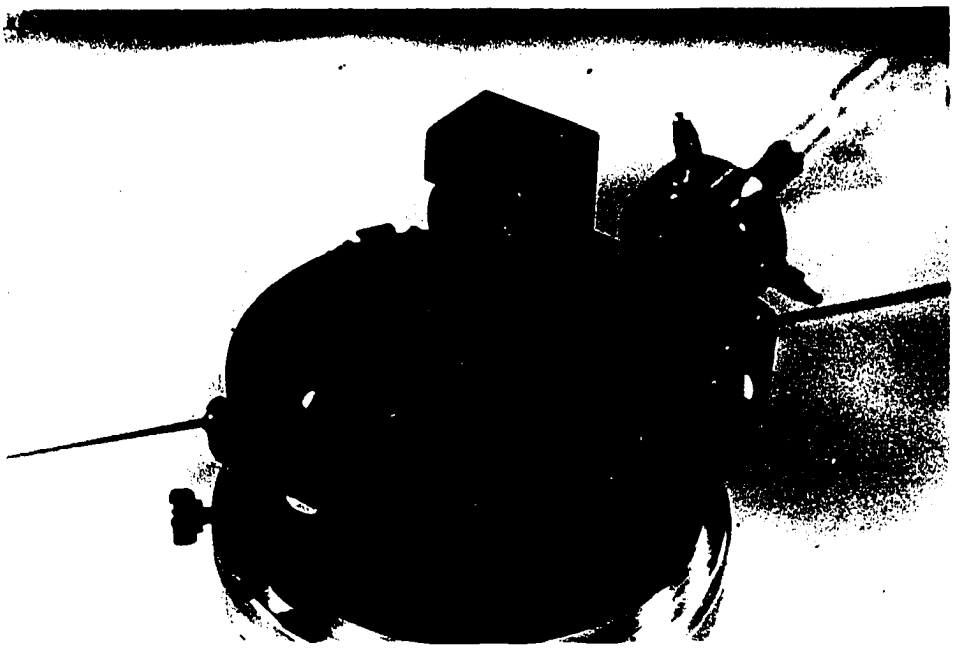

Figure 4. Sample holder with sample for x-ray diffraction study

shown in Figure 5a. The stopcock was fastened securely to a small brass cylinder which was in turn attached to a larger cylinder which fit snugly over the top of the adsorption chamber. Short horizontal slots leading to the holes were filed on the male portion of the stopcock such that very small increments of vapor transfer could be made. The stopcock was provided with a large knurled brass knob for easy manipulation. The tube connecting the adsorption chamber and the stopcock entered the chamber through the gas port fitting of the top cover. Another tube was attached to the exhaust port coupling by a kovar metal tube and supplied the connection between the adsorption chamber and the vacuum train.

At first 0.02 mm aluminum foil alone was used for the X-ray windows. Several times this foil developed pinhole leaks before an adsorption run could be completed. A 1/2 mil "Mylar" polyester film was placed on the inside of the 0.02 mm aluminum foil and no further leakages developed.

The adsorption chamber temperature was controlled by circulating water at constant temperature through the cooling tubes provided in the top and bottom portions of the apparatus. The constant temperature water was also circulated through a cooling coil fastened in a water filled dewar flask such that, when in position, the coil surrounded the water reservoir vapor source. In Figure 5b the flask is shown in the proper position. The constant temperature water source was a thermostat consisting of a polystyrene picnic cooler equipped with a

(a) (b)

Figure 5. Apparatus for x-ray diffraction study (a) without the thermostat for water reservoir, (b) with the thermostat for water reservoir

circulating pump, a motor stirrer, a tap water cooling coil, intermediate and continuous immersion heaters with variable transformer voltage control, a mercury thermoregulator--electronic relay circuit for control of the intermediate heater, and a Beckman thermometer reading to 0.01° C. The temperature of the thermostat was maintained at 22.99° C. The measured temperature in the dewar flask enclosing the water reservoir was 23.2° C during all readings.

The vacuum train was a portable unit consisting of a forepump, an air-cooled oil diffusion pump, a liquid nitrogen cold trap and a Cenco vacuum discharge gauge, all mounted on a rolling cart.

The differences in the mercury levels in the manometer limbs were measured with a Gaertner micrometer slide cathetometer which read directly to 0.001 mm. A general Electric XRD-5 X-ray Diffractometer was used to determine peak positions. Copper Kα radiation with nickel filter was used throughout the test.

Preliminaries

Meniscus correction for observed mercury levels

The mercury levels in the limbs of the manometers were corrected for capillary depression of the apex of the mercury column since meniscus heights were found to differ slightly due to differences in water vapor pressures in the limbs. Data from the International Critical Tables (54) were used to

construct graphs of apex depression versus meniscus height. The meniscus height was measured for each mercury level and the level reading corrected by adding the corresponding apex depression.

Gravity and temperature correction for manometers

Vapor pressure readings were converted to the standard scale by the relation $h_o = \frac{gdh}{g_o d_o}$, where h_o is the corrected manometer reading, d and d_o are the densities of mercury at the test temperature and at 0° C, respectively, g and g_o are local and standard accelerations of gravity. Values of g_o = 980.665 cm/sec^2, d_o = 13.5951 gm/cc, d = 13.5355 gm/cc at 24.36° C and d = 13.5384 gm/cc at 23.2° C were obtained from the literature (34). The local value of acceleration of gravity is g = 980.297 cm/sec^2 (20). Using these values in the above relationship, the following correction values were obtained:

$h_o = 0.9952\ h$ for the adsorption apparatus

$h_o = 0.9954\ h$ for the X-ray apparatus

Procedures

Determination of sorption isotherms

The sodium montmorillonite sample was carefully poured into the sample holder which was then placed in a ground glass stoppered weighing bottle. With the stopper removed, the weighing bottle was placed in a vacuum desiccator containing

phosphorous pentoxide. The desiccator was evacuated with a single-stage forepump and then set aside for several weeks to allow the sample to dry. The vacuum was then released through a phosphorous pentoxide moisture trap and the weighing bottle immediately stoppered. The weighing bottle and its contents were weighed on a certified analytical chain balance; the initial sample weight was found to be 158.7 mg. The sample was then hung on the hangdown loop of the spring balance and lowered into the adsorption chamber. The stopper ("H" in Figure 2) was sealed with mercury. The mercury in the manometer was raised to separate the adsorption chamber from the rest of the apparatus.

Triple distilled water was introduced into reservoir "A" and the end of the tube cut off and sealed with a hand torch. The water was frozen by raising a dewar flask containing a dry ice-acetone mixture around the reservoir. With stopcock "S" open, the frozen water was pumped down to 10^{-5} mm mercury. The stopcock was then closed, the water in "A" thawed to release dissolved gases, refrozen and pumped again. This process for degassing the water was repeated four times.

With stopcock "S" closed, the mercury was lowered in manometer "B" so as to open the adsorption chamber to the rest of the system. The sample was then pumped down to 10^{-5} mm mercury for several days for degassing. After degassing, the mercury was raised in "B", the mercury sealed main stopcock connecting the apparatus to the vacuum train was closed, and

stopcock "S" opened to allow water vapor to enter the right-hand limb of the manometer. The thermostat was filled with water and brought to 24.36°C. When thermal equilibrium was reached, a manometer reading was taken and corrected for temperature, gravity and meniscus. The value obtained agreed with water vapor pressure given in the literature (34).

An initial balance reading under vacuum was made. The mercury was then slowly lowered in the manometer and a small increment of vapor allowed into the adsorption chamber through the manostat arrangement. The mercury was then slowly raised into the manometer limbs. The water reservoir was cooled by raising a dewar flask containing cool water around it to prevent condensation in the right manometer limb while raising the mercury to the proper level. Twenty-four hours was found to be sufficient time for the system to attain equilibrium. Then the pressure difference on the manometer and the spring balance extension were measured. The equilibrium pressure in the chamber was found by making the required corrections on the pressure difference observed and subtracting it from the saturation pressure. The balance extension was converted to mass increase. This was divided by the sample weight to obtain the mass of vapor adsorbed by one gram of montmorillonite. More and more vapor was transferred to the adsorption chamber in the same manner until saturation pressure was attained.

In the vicinity of saturation an additional technique was

used. After the vapor transfer, a small amount of condensation was formed in the upper left limb (chamber side) of the manometer by cooling with a few cubic centimeters of cool water introduced through a pipette. Before saturation this condensation disappeared rapidly. At saturation pressure the time for disappearance increased to several minutes. The mass of vapor adsorbed just before and at saturation differed by less than 0.1 percent.

The desorption isotherm was obtained by condensing more and more vapor back into the water reservoir by cooling it with the dewar flask containing ice water. At relative pressures below about 0.3 the sample was pumped.

Determination of interlayer spacings

A small amount of the sodium montmorillonite was dispersed in distilled water. The dispersion was then pulled, by a water aspirator, through a 30 mm diameter medium porosity fritted glass disc such that a thin layer of the clay was deposited on the disc. The sample was set aside to dry for a day and then was placed in a desiccator containing phosphorous pentoxide. The desiccator was evacuated and set aside for several days to allow the sample to dry. The disc containing the sample was placed in the sample holder and the top of the apparatus was positioned. Triple distilled water was introduced into the water reservoir which was then attached to the apparatus. With the stopcock connecting the reservoir and

adsorption chamber closed, the water in the reservoir was frozen by immersing in a dry ice-acetone mixture. The stopcock was opened and the frozen water and sample pumped to about 10^{-3} mm Hg. Then the stopcock was closed and the ice melted to release dissolved gases. This process for degassing the water was repeated four times. The stopcock was then kept closed while the sample was pumped each day for two weeks. The lowest vacuum attained, as registered on the Cenco discharge vacuum gauge, was 10^{-4} mm Hg. The connection between the adsorption chamber and the vacuum train was cut and sealed with a torch. The apparatus was then connected to the constant temperature water circulation system, placed on the X-ray diffractometer and the sample aligned according to the procedures given by the manufacturer of the high temperature attachment. When thermal equilibrium was attained the sample was X-rayed with copper Kα radiation and a trace of the initial 001 peak obtained; this was repeated until five traces of the peak were taken. A manometer reading was taken and corrected for temperature, gravity and meniscus. The value obtained agreed with water vapor pressure given in the literature (34). The initial 001 peak was at a spacing of 9.8 Å.

After getting initial peak and pressure readings, the stopcock was partially opened to allow a small increment of water vapor into the adsorption chamber. After a period of 24 hours the pressure differences on the manometer and the new position of the 001 peak were observed. Each new peak

position was recorded five times. The equilibrium pressure in the adsorption chamber was calculated as before. In this manner more and more water vapor was transferred to the chamber until the saturation pressure was reached. Desorption was accomplished by condensing more and more vapor back into the water reservoir by cooling it with ice water until a p/p_o of about 0.3 was reached. For values of p/p_o from 0.3 to about 0.03 the desorption was accomplished by freezing the water in the reservoir with a dry ice-acetone mixture. For the last increment the apparatus was connected to the vacuum train and pumped for two-and-one-half days and then placed on the X-ray unit for the final readings.

Errors

Experimental error in determining p/p_o

The error in determining p/p_o for the adsorption apparatus was calculated for earlier studies and found to be ± 0.003 for all pressure ranges (20,58).

For the X-ray study apparatus, the reproducibility of pressure difference readings with the cathetometer was found to be within ± 0.05 mm. The maximum error in the value of p_o due to temperature variations was estimated to be ± 0.13 mm Hg. The error in p/p_o was calculated from the relationship (60, p. 20):

$$\left(\delta\frac{p}{p_o}\right)^2 = \left(\delta\frac{p_o - \Delta p}{p_o}\right)^2 = \left(\delta\frac{\Delta p}{p_o}\right)^2 = \left(\frac{\partial\frac{\Delta p}{p_o}}{\partial\Delta p}\delta\Delta p\right)^2 + \left(\frac{\partial\frac{\Delta p}{p_o}}{\partial p_o}\delta p_o\right)^2$$

from which:

$$\delta\frac{p}{p_o} = \pm\left[\left(\frac{\delta\Delta p}{p_o}\right)^2 + \left(1 - \frac{p}{p_o}\right)^2\left(\frac{\delta p_o}{p_o}\right)^2\right]^{1/2}$$

where $\delta\frac{p}{p_o}$, δp_o and $\delta\Delta p$ are the errors in p/p_o, p_o and the pressure difference, respectively. The calculated errors in p/p_o for various pressure ranges were as follows: ± 0.007 for $0 \leq p/p_o < 0.1$, ± 0.006 for $0.1 < p/p_o < 0.3$, ± 0.005 for $0.3 < p/p_o < 0.5$, ± 0.004 for $0.5 < p/p_o < 0.7$ and ± 0.003 for $0.7 < p/p_o < 1.0$.

Experimental error in determining q

The weight of adsorbate, q, in grams per gram of adsorbent was calculated from $q = \frac{LS}{10^3 W}$, where L is the spring balance extensions in optical reader divisions, S is the balance sensitivity in milligrams per optical reader division and W is the sample weight in grams. From the reproducibility of spring balance extension and the estimated errors in balance sensitivity and sample weight, the error in q was calculated to range from ± 5 x 10^{-5} gm/gm in the low pressure range to ± 4 x 10^{-4} gm/gm near saturation pressure for an earlier study. For the present study, similar calculations

for a more sensitive balance, but for a smaller sample, gave corresponding values of $\pm$ 3 x 10^{-5} gm/gm and $\pm$ 3 x 10^{-4} gm/gm. However, it is felt that these estimations are conservative since possible relative movements of components of the adsorption apparatus and errors in resetting the zero point of the optical reader (although probably small) could not be included.

PRESENTATION AND DISCUSSION OF RESULTS

X-ray Diffraction

The data from the X-ray diffraction study of sodium montmorillonite during adsorption and desorption of water vapor are presented in Tables 2 and 3, and Tables 4 and 5 for the first and second cycles, respectively. A discussion of the experimental error in determining values of p/p_o was presented earlier. The values tabulated for the basal spacings, line widths and intensities (based on peak heights) are the average of five observations for each determination. The accuracy with which individual observations could be made was dependent on the size of the diffraction angle and on the sharpness of the peaks obtained, which varied with different regions of relative pressure. The average variation from the average value for five observations of the basal spacing were less than ± 0.10 Å, with a maximum variation of ± 0.25 Å at small angles; for line widths the variations were from ± 0.01 to ± 0.10 degrees. Variations of measured intensities (peak heights) were from ± 4% to a maximum of ± 18% with an average variation of about ± 10%. The line widths of the diffraction peaks obtained were determined as sketched in Figure 6. The values thus obtained and the first order basal spacings are plotted against the relative pressures at which they were observed in Figure 7. The solid curves represent data from the first cycle and the dashed curves represent the second cycle.

Table 2. X-ray diffraction data, first adsorption run

p mm Hg	p_o mm Hg	p/p_o	Basal spacing, d_{001}, Å	Line width, B_o, degrees	Intensity, H
0	21.34	0	9.82	0.84	6.2
1.35		0.063	9.83	0.87	6.4
3.03		0.142	9.81	1.07	4.0
3.74		0.175	9.82	1.16	3.6
4.58		0.215	9.93	1.43	3.4
5.45		0.255	10.01	1.56	4.0
5.79		0.271	10.11	1.90	4.6
7.24		0.339	10.77	2.27	5.0
9.13		0.428	11.70	1.89	9.1
9.74		0.456	11.94	1.64	9.8
10.38		0.486	12.22	1.47	10.8
11.00		0.515	12.18	1.39	12.0
12.85		0.602	12.44	1.10	16.4
14.58		0.683	12.62	1.10	15.6
16.69		0.782	14.13	1.56	12.7
17.77		0.833	14.84	1.29	16.8
18.75		0.879	15.28	1.05	20.8
19.28		0.903	15.41	0.98	21.6
20.20		0.947	15.57	0.92	21.9
20.75		0.972	16.02	1.20	20.5
20.87		0.978	16.23	1.27	20.0
20.87		0.978	16.50	1.28	18.4
20.81		0.975	16.75	1.35	25.0
21.03		0.985	17.98	1.32	26.6
21.04		0.986	18.02	1.44	28.7
21.07		0.987	18.05	1.33	25.4
21.32		0.999	18.20	1.46	32.8

Table 3. X-ray diffraction data, first desorption run

p mm Hg	p_o mm Hg	p/p_o	Basal spacing, d_{001}, Å	Line width, B_o, degrees	Intensity, H
19.42	21.34	0.910	17.66	1.51	30.1
18.96		0.888	17.66	1.52	29.6
18.38		0.861	17.66	1.50	32.4
15.87		0.744	16.29	1.52	30.2
14.03		0.657	16.00	1.16	34.5
12.15		0.569	16.02	0.96	38.1
9.28		0.435	14.98	1.62	19.9
7.48		0.351	12.82	1.66	16.1
7.05		0.330	12.62	0.78	24.2
2.11		0.099	11.01	1.84	5.4
0.81		0.038	10.13	1.32	5.5
0		0	9.96	--	6.8

Table 4. X-ray diffraction data, second adsorption run

p mm Hg	p_o mm Hg	p/p_o	Basal spacing, d_{001}, Å	Line width, B_o, degrees	Intensity, H
0	21.34	0	9.96	--	6.8
3.22		0.151	10.04	1.50	8.8
5.50		0.258	11.44	2.54	9.2
8.58		0.402	12.37	1.47	22.1
11.05		0.518	12.39	1.24	16.4
13.36		0.626	12.82	1.72	18.1
16.39		0.768	14.94	1.29	27.8
19.12		0.896	15.77	0.98	31.5
19.29		0.904	15.77	0.98	35.8
20.85		0.977	17.14	1.54	30.3
21.34		1.000	18.67	1.05	36.0

Table 5. X-ray diffraction data, second desorption run

p mm Hg	p_o mm Hg	p/p_o	Basal spacing, d_{001}, Å	Line width, B_o, degrees	Intensity, H
15.15	21.34	0.710	16.05	1.34	28.3
10.76		0.504	16.00	1.35	30.0
6.38		0.299	12.76	1.12	16.2
4.29		0.201	11.78	1.55	16.0
0.28		0.013	9.95	1.18	5.2

Perhaps the most obvious feature of the plot is the shift of the adsorption curve for the second cycle from the position of that for the first. The same behavior was observed with an earlier sample used in incompleted runs. With the earlier sample, the first adsorption curve followed the present one very closely up to a p/p_o of 0.70. The X-ray window then developed a leak and had to be repaired. The next try with the same sample was shifted to a position between those shown in Figure 7, somewhat closer to the curve for the second run. Another leak in the X-ray window terminated this run at a p/p_o of 0.45. After solving the leakage problem a new sample from which the present data was obtained was placed in the apparatus.

The reason for the observed shift in position of the adsorption curve is not clear. Figure 7 shows the initial average basal spacing was not attained on desorption,

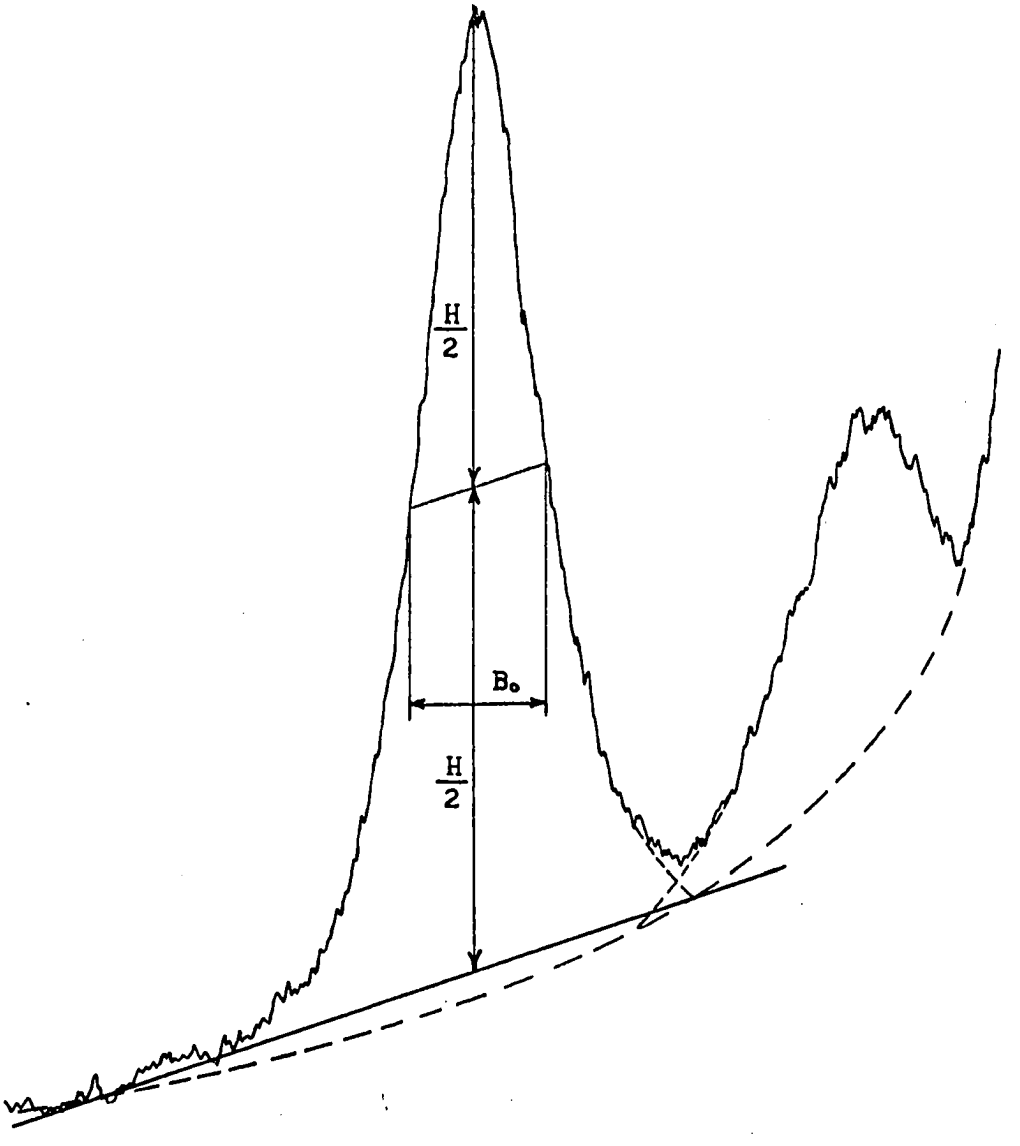

Figure 6. Method of determining line widths and peak heights of X-ray diffraction peaks

Figure 7. Variations of first order basal spacings and line widths with relative pressure of water vapor for sodium montmorillonite

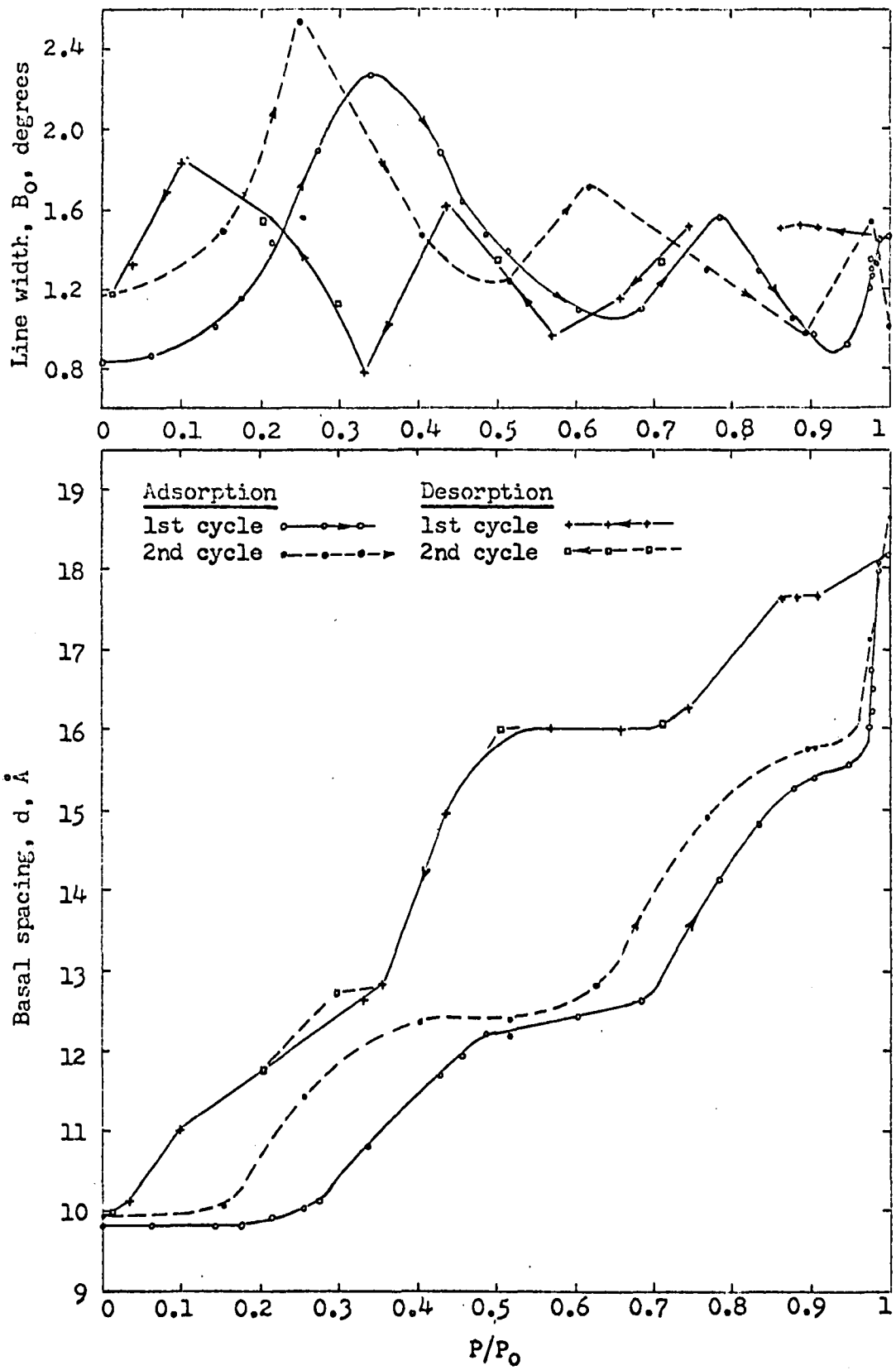
Line width, B_o, degrees
2.4
2.0
1.6
1.2
0.8
0
0.1
0.2
0.3
0.4
0.5
0.6
0.7
0.8
0.9
1
Adsorption
1st cycle
2nd cycle
Desorption
1st cycle
2nd cycle
Basal spacing, d, Å
19
18
17
16
15
14
13
12
11
10
9
P/P_o

indicating some water was left entrapped in the interlayer regions. Perhaps this remaining water, with the accompanying greater average spacing, affected the platelet interactions such that separation of the layers could more readily occur, as shown by the second curve which was started after a brief period of degassing. Although improbable, there may have been a remote possibility of contamination of the sample while in the adsorption chamber.

Since the initial adsorption curves for two samples were very nearly the same, and since the procedure for reaching the initial sample condition was the same as in the adsorption isotherm study, it is felt that the X-ray data for the first adsorption run are more dependable than those for the second run. Therefore, discussions in this report will be based primarily on the initial adsorption curve for X-ray data. The general trends for the two runs, except for the shift in position, are the same.

Hendricks and Jefferson (31) have shown that theoretically the X-ray diffraction from a powder should show that the basal spacing would vary continuously with water content. Hendricks et al. (32) found this to be so in their study. Mooney et al. (52), from X-ray data on desorption from Wyoming montmorillonite and data of Hendricks et al. (32) on Mississippi and California montmorillonites produced an almost perfect stepwise curve. However, as will be discussed later, there was considerable scatter of the data, especially for

Hendricks' Wyoming montmorillonite (which was ignored by Mooney et al.) for which only diffuse diffraction bands were observed.

The data of the present study, Figure 7, shows that the change in average basal spacings takes place in a continuous but non-uniform manner with changes in relative pressure. The continuity is apparently due to the existence, simultaneously, of varying numbers of molecular layers of water, i.e. 0, 1, 2, ... , between clay platelets. The plot of line width versus relative pressure substantiates this conclusion. The variations in widths of the observed diffraction peaks are in part due to the lack of constancy of interlayer spacings (40, p. 517) and give an indication of the relative amount of layers at the various spacings (44). The adsorption curve of Figure 7 shows that the line width increases somewhat at low relative pressures, indicating some uptake of water in the interlayer regions although the average basal spacing remains constant at about 9.8 Å. As the basal spacing increases there is a corresponding increase in line width to a maximum occurring near the center of the steeper portion of the basal spacing plot. The line widths then decrease as the basal spacing plot approaches a flatter portion. A minimum line width is reached which corresponds to a basal spacing on the flat portion of the curve. The minimum line width indicates that most of the clay platelets are nearly at the observed spacing. As the relative pressure increases another increment

of expansion takes place and the line widths follow the same pattern as described above. Water take-up continues in this manner until the saturation pressure is reached.

Data for the desorption runs was not extensive enough to determine the shapes of the curves of Figure 7 as well as could be done with adsorption data. The data for basal spacings and line widths were fairly close for the two cycles and the desorption curves of Figure 7 were sketched using the data for both cycles. The general trends and relationships between line widths and basal spacings are similar to those discussed for the adsorption curves.

The heights of the diffraction peaks obtained were determined as sketched in Figure 6. As discussed earlier, the variations from the average for some determinations were as much as ±18%, the average variations being about ±10%. The quality of the present intensity data does not permit more than a rough qualitative analysis. The integrated intensity of a diffraction peak is basically more sound than is the peak height (11). Since all of the peaks obtained were roughly triangular in shape, an approximation of the peak area was made by multiplying the peak height by the peak width. The values thus obtained for the first adsorption-desorption cycle are plotted against relative pressures in Figure 8. In general, the intensity increases as water is adsorbed and the basal spacing increases. This is consistent with the observations of others (37,50). Johns, Grim and Bradley (37) have

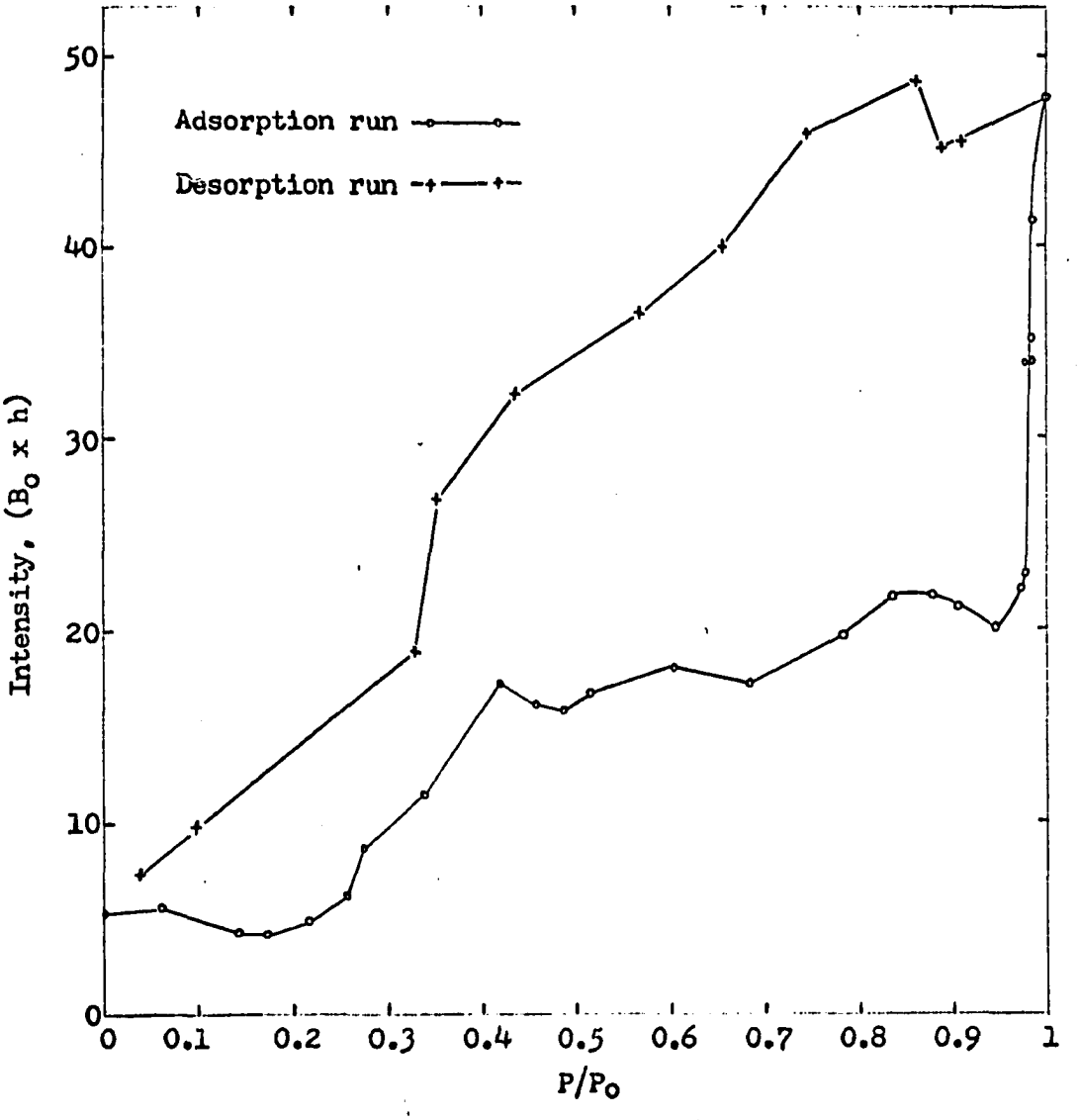

Figure 8. Variation of intensity (B_o x h) of X-ray diffraction peaks with relative pressure of water vapor for sodium montmorillonite

shown that the intensity of diffraction from three-layer clay minerals at an angle corresponding to 17 Å should exceed that reflected at 10 Å by a factor of approximately four. Comparison of basal spacing data, Figure 7, and intensity data, Figure 8, for the adsorption run shows that this is roughly true with the present data. The intensity of diffraction is given by $I = \theta \left| F_1 \right|^2 \Phi$, where θ is the combined Lorentz-polarization factor which increases with decreasing diffraction angle, F_1 is the layer structure factor which increases with increased spacings, and Φ is the mixing function dependent on the spacings of the constituent phases and the probability of occurence of these spacings (44). According to MacEwan, Amil and Brown (44), water molecules between clay layers will have only a minor effect on the structure factor F_1. The Lorentz-polarization factor θ alone would cause a 17 Å peak to be nearly three times as intense as a 10 Å reflection (40, p. 683). Local maxima and minima of observed intensities are probably due to the mixing function Φ, i.e. the relative proportions of layers at different spacings and the randomness of their distribution.

Comparison with data of other investigators

Figure 9 presents the basal spacing versus relative pressure data of Hendricks et al. (32), Mooney et al. (52), Gillery (27), Demirel (20) and Messina (48) for various sodium montmorillonites. Considerable scatter of the reported data

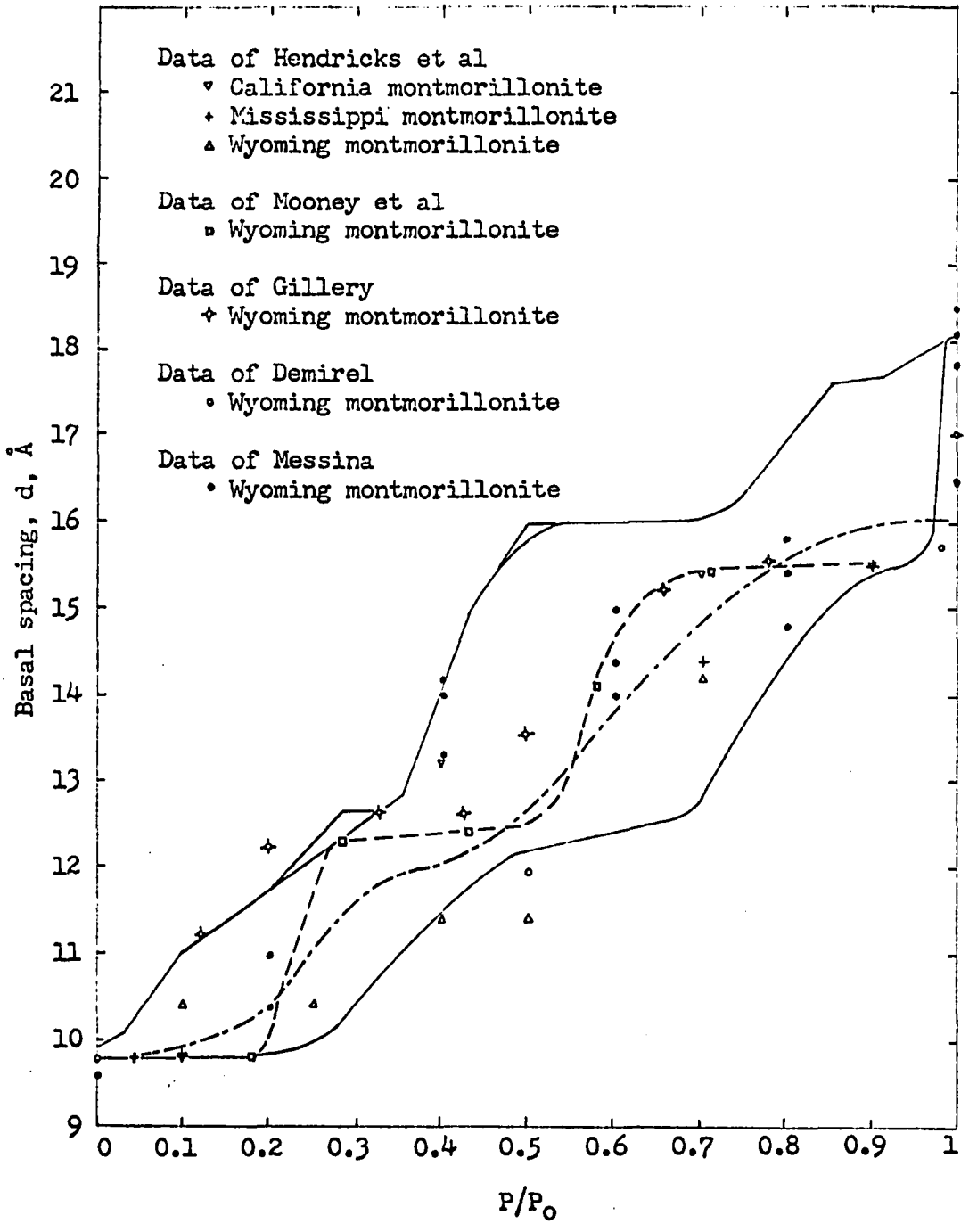

Figure 9. Variations of first order basal spacings with relative pressure for sodium montmorillonites as reported by various investigators

is apparent. The solid curves trace the first adsorption-desorption cycle of the present study. This loop encloses most of the data presented; exceptions are one point for Hendricks' Wyoming montmorillonite, two points from Demirel's data, and several of Gillery's and Messina's values at saturation pressure. The stepwise dashed curve is that presented by Mooney et al. (52); the other dashed curve is an average proposed by Demirel (20) for his data and that of Hendricks and of Mooney.

There are probably several reasons for the observed scatter of data reported. It is felt that the history of the sample would have a definite effect on the results obtained. The history of the sample includes its source, method of preparation, test procedures, etc. Other factors may be the degree of temperature and humidity control and the interpretation of diffuse diffraction bands or peaks.

Hendricks et al. (32) used montmorillonites from California, Mississippi and Wyoming. The Wyoming material was a Wyoming bentonite sold under the trade name "Volclay". Mooney et al. (52) used a Wyoming bentonite, Volclay-SPV, obtained from the American Colloid Company. Both groups prepared the sodium clay by titrating suspensions of the electrodialyzed clay with NaOH to a specific pH, 8 for Hendricks et al. and 7.5 for Mooney et al. Gillery used a natural Wyoming bentonite supplied by the National Lead Company; he does not state whether it was treated to assure it was

homoionic. Messina's material was a Wyoming bentonite but the source was not given. It was treated with NaCl solutions for the conversion of the interlayer cation to sodium. The material used by Demirel, and in the present study, was a Wyoming bentonite, Volclay-SPV, produced by the American Colloid Company. It was treated with NaCl solutions to obtain a homoionic material as discussed earlier.

Mooney et al. (52) used the data of Hendricks et al. (32) and their own to determine the stepwise curve presented in Figure 9. The test procedure in the two studies were quite different. Hendricks et al. used initially dry samples (dried over phosphorous pentoxide in vacuum) which were exposed at 30° C to water vapor, at various relative humidities ranging from 0.05 to 0.90, for a week or longer to attain equilibrium. Mooney et al. used samples taken from their adsorption apparatus during desorption at 20° C, apparently 24 hours being allowed for attainment of equilibrium between vapor transfers. In their first paper Mooney et al. (51) found that the desorption isotherms were reproducible provided the adsorption curve was carried up as high as the final steeply-rising section. In their second paper (52, Figure 4) the first point of their desorption curve for sodium montmorillonite is at a p/p_o of about 0.95. Since this is in the range of the final steep portion of the adsorption curve, perhaps they began desorption before saturation pressure was attained. Figures 7 and 9 of the present study show that an additional

increment of layer separation occurs at relative pressures above 0.95; at p/p_o of 0.95 the basal spacing observed was 15.6 Å. If Mooney et al. began their desorption at a relative pressure of 0.95, their curve should begin at this spacing. Figure 9 shows that the initial flat portion of their desorption curve is at 15.5 Å. Although they did not have an experimental observation at p/p_o of 0.95, they found a spacing of about 15.4 Å at a p/p_o of about 0.70. They also used some of Hendricks et al. data to determine the curve in this region. These were 15.4 Å and 15.5 Å at relative pressures of 0.70 and 0.90, respectively, for California montmorillonite, and 15.5 Å at a p/p_o of 0.90 for Mississippi montmorillonite. The low position of Mooney's desorption curve as compared to that of the present study may, therefore, be due to failure to attain saturation pressure and the final increment of expansion on adsorption. This, as well as the shift in the adsorption curve due to insufficient desorption as discussed earlier, would seem to demonstrate the importance of the initial conditions of the sample.

Hendricks et al. and Mooney et al. controlled the temperature during equilibration of their samples. Mooney et al. used manometer measurements to determine the relative pressure within their adsorption apparatus. Hendricks et al. did not discuss the accuracy of the relative humidities reported nor the procedure used to maintain a specific value. Both groups sealed their X-ray samples in small glass capillary tubes to

prevent loss of water and used X-ray cameras for diffraction measurements. Neither group discusses temperature control during the 10 to 48 hour period of exposure to X rays. The relative humidities reported were those determined while the samples were in the adsorption chamber or desiccator. Temperature changes would effect the relative pressures within the sample tubes and may account, to some degree, for the scatter in the reported data.

Gillery (27) controlled the relative humidity during exposure to X rays by passing compressed air through appropriate saturated salt solutions and into the sample chamber; humidities were measured with wet and dry thermocouples. His data were taken during desorption. Messina (48) equilibrated his samples at certain relative humidities in a desiccator. Humidity control during exposure to X rays was similar to the method used by Gillery. Messina does not state whether the data was collected during desorption or during adsorption. Neither party discusses temperature control during testing. Messina's data points out another factor causing differences in the observed data. He used four particle size fractions in his study; 2 to 1 micron, 0.4 to 0.3 micron, 0.15 to 0.05 micron and less than 0.05 micron. Messina attributed the scatter of his data (Figure 9) to the size of the particles; at low humidities clays with high charge densities, the coarse fractions, expanded the most because of cation or silicate layer hydration and at high humidities the coarse fractions

expanded the least because of strong binding forces between layers while the fine fractions, with lower charge densities, expanded more because of weaker binding forces and the strong adsorption force of water molecules. He used the argument of selective cation removal at the edges of small particles for a possible reduction of ion density, hence charge density. Jonas and Roberson (38) concluded that coarse particles would retard expansion because of the large flake area furnishing sites for a large number of interlayer ions; when large numbers of such cations are present, regardless of their density per unit area, expansion is retarded.

Demirel (20) equilibrated his initially dry samples, at room temperature, in vacuum desiccators maintained at the desired relative humidities by appropriate saturated salt solutions. During exposure to X rays the sample and appropriate solution were covered by a plexiglass hood equipped with Mylar X-ray windows. Since the humidity above the solutions is dependent on temperature the actual relative humidity would vary somewhat with changes in room temperature. Considering the differences in procedure, the data of Demirel is in quite good agreement with the adsorption data of the present study. Since the material used in the two studies was the same, this would seem to demonstrate the importance of the source of the material and the method of preparation.

Summing up the discussion of X-ray data presented in the literature, it is concluded that the major factors responsible

for the scatter observed are: a) the initial conditions of the sample at the start of the test, b) the source and method of preparation of the material, and c) whether the data is collected during adsorption or desorption. Other factors are the control of temperature and humidity and possibly the size of the particles present. In correlating X-ray results with other methods of investigation care should be taken to assure that the material and test conditions are as nearly the same as possible.

Arrangement of interlayer water

As adsorption on the internal surfaces of montmorillonites proceeds the molecular layers of water build up either in laminae or in another spatial geometric arrangement. In the first case the stable thicknesses should be integral multiples of the diameter of a water molecule; in the second they should conform to the geometry and the size of the water molecules. Hypothetical configurations for the water adsorbed on the clay surface have been postulated by several investigators (30, p. 162).

Hendricks and Jefferson (31) hypothesized that an extended hexagonal net of water molecules is hydrogen bonded to the clay mineral surface. Successive hexagonal nets build up on each other by being hydrogen bonded to the previous one. Taking 2.76 Å as the thickness of a water molecule (56, p. 464), their hypothesis results in a laminated stacking causing

a separation of 2.76 Å for each molecular layer of water. Each water molecule in a layer covers an area of about 11.5 $Å^2$.

Macey (42) noted the lattice similarities between the basal planes of ice and of clay minerals. He suggested the ice structure develops on clay mineral surfaces with the hexagonal molecular configuration of the basal plane of ice. This structure tends to build outward from the surface. Demirel (20) presents two ways in which the ice structure may develop in the interlayer regions. One would be to stack the hexagonal rings in the way they successively occur in the quartz-like structure of ice. This would cause an alternating platelet separation of 2.76 Å and 0.92 Å with successive molecular layers of water. In the second method the first hexagonal network is shared by two montmorillonite platelets causing a separation of 2.76 Å; two hexagonal networks are stacked and held by the two silica surfaces causing a separation of 5.52 Å; the third and fourth molecular layers of water fill in between the hexagonal networks forming tetrahedrons with the water molecules of the network. A complete unit cell of ice is formed with the entrance of the fourth molecular layer of water, causing a separation of 7.36 Å. The fifth and sixth layers of water enter between the unit cell of ice and the clay surfaces, forming hexagonal networks and causing separations of 10.12 Å and 12.88 Å, respectively. Demirel (20), using data reported in the literature and his own for various species of homoionic montmorillonites, found evidence

to support the build up of an ice structure in the second way. With an ice structure, the area covered by a water molecule is about 17.5 $Å^2$.

Forslind (23,24) suggested the same ice structure arrangement postulated by Macey but based his argument on the Edelman-Favejee structure (43, p. 152) rather than the Hofmann-Endell-Wilm structure of montmorillonite (43, p. 146).

Barshad (6) suggested an arrangement which becomes progressively denser with addition of monomolecular layers of water. He postulated several possible arrangements for the water molecules. There are two alternative arrangements for the first layer; the molecules may form tetrahedra with the basal oxygens of the clay surface and cause a separation of 1.78 Å, or the centers of the water molecules may be vertically above and below the centers of the oxygens and cause a separation of 2.76 Å. When two molecular layers of water are present, three possible separations may occur depending on the superimposition of water molecules on the oxygens of the clay surface and the superimposition of the water layers. If the water molecules form tetrahedra with the basal oxygens and octahedra at the water-water interface the separation is 1.78 + 2.09 = 3.87 Å. If they form tetrahedra with oxygens but are vertically above each other at the water-water interface the separation is 1.78 + 2.76 = 4.54 Å. If they are vertically above the basal oxygens and each other the separation is 2.76 + 2.76 = 5.52 Å. Similarily, there are three possible

separations when three molecular layers of water are present; namely 5.96, 7.30 and 8.28 Å. Depending on the arrangement of the water molecules at the clay surface, the area covered per molecule will be about 11.5 $Å^2$ or about 7.7 $Å^2$.

The continuity of the basal spacing versus relative pressure curve has been attributed to the simultaneous existence of clay platelets separated by various molecular layers of water. If all of the interlayer water has been removed at zero relative pressure, a sharp peak will be observed corresponding to the collasped basal spacing of sodium montmorillonite, about 9.60 Å (12). As the relative pressure increases some water begins to penetrate between some of the clay layers. If it is assumed that the system consists primarily of layer spacings corresponding to zero and one molecular layers of water between platelets, i.e., that the contributions of layers separated by 2, 3 or more molecular layers of water to the observed diffraction peaks are negligible, then the system may be treated as a random interstratification of two components. The basal spacing of one of these components corresponds to that with zero molecular layers of water between clay platelets; that of the other component corresponds to the spacing when one molecular layer of water is present. In a similar manner observed peaks corresponding to separations between those for one or two molecular layers of water may be treated as a composite peak from another random two component system, i.e., one component

corresponding to one molecular layer of water and the other to two such layers. This may be extended to higher increments of expansion. As the relative pressure increases, the relative proportions of the two components change and the observed diffraction peaks migrate from the position of the first pure component, A, toward that of the other pure component, B. According to MacEwan, Amil and Brown (44), in a preliminary analysis there will be no great error in assuming that the peaks move linearly between the two pure component positions. When the distance from the observed peak to the A and B positions are x and y, respectively, the proportion of component A is deduced to be $y/(x + y)$. As the observed peak migrates from the A position it first becomes diffuse and then sharper again as it approaches the B position. Taking the line width to be a function of the non-constancy of layer separations, we would suspect that a maximum width would correspond to the most random distribution of the different layer separations and that this would occur when the relative proportions of the two components are nearly equal. Although this conclusion may not be strictly true (44), it is felt that assuming the maximum line width corresponds to an A/B ratio of one will be in no greater error than that in assuming the peak migration to be linear.

If it is assumed that a) the system of the present study may be treated as a random interstratification of two components, b) peak migration between pure component positions is

linear and c) maximum line widths occur when the relative proportions of the two components are equal, the line width and basal spacing data of this study may be used to test possible arrangements for the interlayer water that have been postulated by various investigators. The minimum line widths should correspond to a basal spacing near that calculated from the proposed arrangement for an integral number of molecular layers of water between clay platelets. If assumptions b and c hold, the maximum line widths should occur at a basal spacing which is the average of those calculated for two successive molecular layers of water between platelets, i.e. midway between the positions for 0 and 1 layers of water, or 1 and 2 layers, etc.

Using 9.60 Å as the collapsed basal spacing of sodium montmorillonite, the basal spacings for integral molecular layers of water between platelets, as calculated from the postulated interlayer water structures discussed earlier, and the averages of each two successive spacings are presented in Table 6. The observed basal spacings and line widths for the first adsorption run are plotted against one another in Figure 10. Comparison of Table 6 and Figure 10 shows that the laminated structures and the second suggestion for an ice structure give the best correlations for sodium montmorillonite. The first maximum line width occurs at a basal spacing of about 11.0 Å, very near the 10.98 Å average calculated for zero and one molecular layers of water. The first minimum

Table 6. Calculated first order basal spacings of sodium montmorillonite for various suggested interlayer water configurations

Number of molecular layers of water	Configurations resulting in laminated stacking[a,b]		Ice configurations[c]			
			Alternative No. 1		Alternative No. 2	
	Calculated basal spacing, Å	Average, two successive spacings, Å	Calculated basal spacing, Å	Average, two successive spacings, Å	Calculated basal spacing, Å	Average, two successive spacings, Å
0	9.60		9.60		9.60	
		10.98		10.98		10.98
1	12.36		12.36		12.36	
		13.74		12.82		13.74
2	15.12		13.28		15.12	
		16.50		14.66		13.74
3	17.88		16.04		15.12	
		19.26		16.50		16.04
4	20.64		16.96		16.96	
		22.02		18.34		18.34
5	23.40		19.72		19.72	
		24.78		20.18		21.10
6	26.16		20.64		22.48	

[a]Configuration of Hendricks and Jefferson (31).

[b]Third alternative of Barshad (6).

[c]Alternatives suggested by Demirel (20).

Table 6. (continued)

Number of molecular layers of water	Other configurations[d]			
	Alternative No. 1		Alternative No. 2	
	Calculated basal spacing, Å	Average, two successive spacings, Å	Calculated basal spacing, Å	Average, two successive spacings, Å
0	9.60		9.60	
		10.49		10.49
1	11.38		11.38	
		12.43		12.76
2	13.47		14.14	
		14.52		15.52
3	15.56		16.90	

[d]First and second alternatives of Barshad (6).

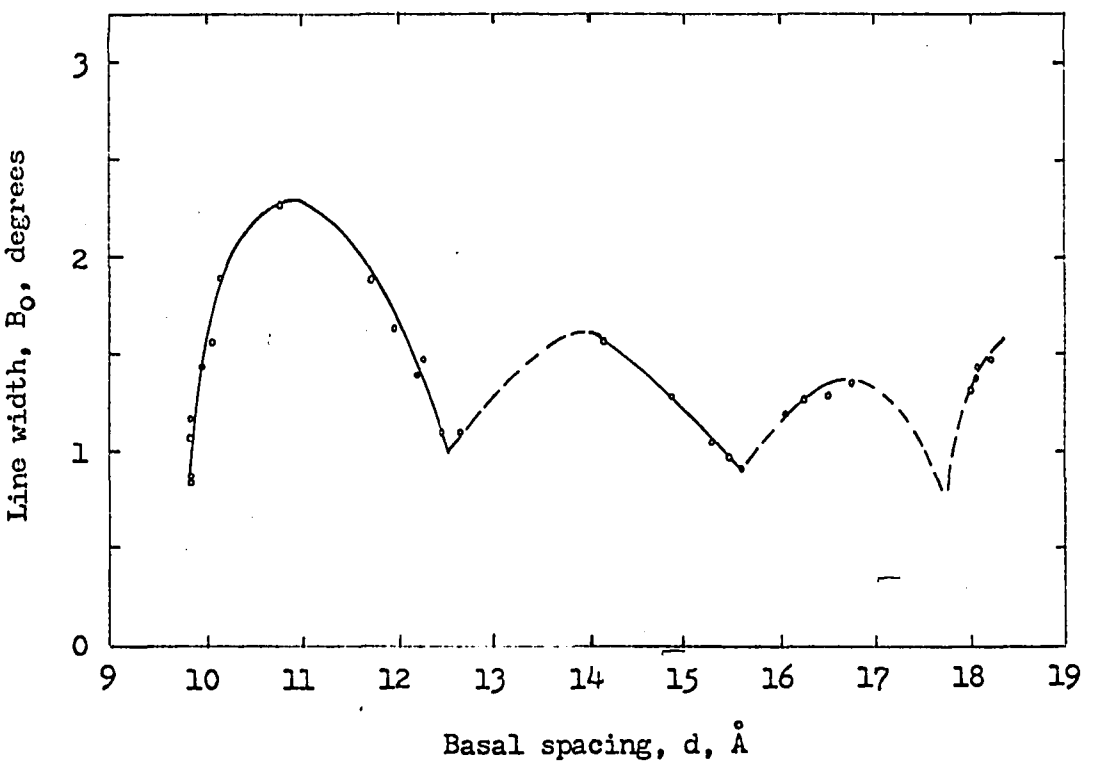

Figure 10. Variation of line widths with basal spacings of sodium montmorillonite

line width occurs at about 12.5 Å which is close to the calculated value of 12.36 Å for one molecular layer of water. Although the observed data is scarce, the second maximum line width appears to be at about 14 Å which is reasonably near the 13.74 Å average for one and two layers of water. The second minimum line width is at about 15.5 Å, somewhat higher than the 15.12 Å calculated for two layers of water. The higher than expected basal spacings corresponding to the observed line width minima may be due to failure of the assumption of a two-component system in the region near the peak position for a pure component (all platelets at one spacing). As the peak position approaches that for a pure component the number of platelets at the next increment of expansion increase and most probably their contributions to the observed peak are no longer negligible. Therefore, the system in this region is likely to be one of three rather than two components and the observed minimum line width may well occur at a slightly higher average basal spacing.

The rest of the data plotted in Figure 10 are not very conclusive. Figure 7 shows that the data in this region are all in the p/p_o range of 0.97 to 1.00 and are quite crowded. However, Figure 10 does show that a probable maximum line width does occur at a basal spacing greater than about 16.7 Å. This is closer to the 16.5 Å average calculated for laminated structures than it is to the 16.04 Å average for the ice structure. The last group of points in Figure 10 suggest a

minimum line width may occur at an average basal spacing of slightly less than 18 Å. Again, this is nearer the 17.88 Å calculated for three molecular layers of water in a laminated structure than it is to the 16.96 Å calculated for four molecular layers of water in an ice structure. More extensive data at high relative pressures are needed for a definite conclusion to be drawn. With the present apparatus the relative pressures can be determined within ±0.003 in this region as discussed earlier, so smaller increments of vapor transfer would not add much to the basal spacing-relative pressure relationship obtained at high relative pressures in this study. However, smaller increments at high relative pressures may enhance the line width-basal spacing relationship in this region.

The data of this study gives evidence of the formation of a laminated arrangement of the interlayer water rather than an ice structure for sodium montmorillonite with up to three layers of water. Whether the arrangement in individual layers of water would be as suggested by Hendricks and Jefferson (31), Barshad's third alternative (6), or in some other manner can not be ascertained from this data. More detailed studies with sodium montmorillonite, and with other materials such as calcium montmorillonite, may give more complete evidence. Also, better data on the intensity of diffraction peaks may be helpful. Other methods of investigation, e.g. nuclear magnetic resonance studies, heat capacity studies, etc. may also

enable more definite conclusions to be drawn.

Sorption Isotherms

The data for adsorption and desorption and the values of the functions for evaluation of BET parameters and energy changes are presented in Tables 7 and 8, 9 and 10, and 11 and 12 for the first, second and third cycles, respectively.

Figure 11 is a plot of the sorption isotherms. The adsorption and desorption branches fall in different regions of the plot, illustrating the hysteresis expected with porous adsorbents (13,25,45). It may be seen that the desorption branches for the first and third runs do not come back to the initial q value, but that the desorption branch of the second run does attain this value. In Tables 9 and 10, the values of the functions $\frac{p}{q(p_o-p)}$ and $\frac{q}{p/p_o}$ shown were computed from the isotherm beginning at q equal to zero rather than the value reached on the first desorption run.

In their study of water vapor adsorption by montmorillonite, Mooney et al. (51,52), on the basis of irreversible hysteresis, assumed that the desorption branch represented the true equilibrium curve. This is consistent with the theory proposed by Zigsmondy if the irreversibility of hysteresis persists in succeeding adsorption-desorption runs, and if incomplete wetting due to surface impurities is the only cause of hysteresis (13, p. 394; 1, p. 524). Mooney et al. (51) found that the desorption branch was more closely reproduced

Table 7. Adsorption isotherm data, first cycle

p mm Hg	p_o mm Hg	p/p_o	q, $\frac{gm}{gm} \times 10^3$	$\frac{p}{q(p_o-p)}$	$\frac{q}{p/p_o}$
0.14	22.87	0.006	5.10	1.21	0.850
0.38		0.017	7.81	2.16	0.459
0.50		0.022	9.08	2.46	0.413
1.34		0.059	12.44	5.00	0.211
2.57		0.112	16.33	7.75	0.146
3.44		0.150	19.26	9.19	0.128
4.09		0.179	22.09	9.86	0.123
4.91		0.215	25.72	10.63	0.120
5.93		0.259	32.21	10.87	0.124
6.82		0.298	40.48	10.50	0.136
8.09		0.354	56.08	9.76	0.158
9.73		0.425	72.48	10.22	0.170
11.30		0.494	87.78	11.13	0.178
13.63		0.596	115.8	12.74	0.194
15.21		0.665	146.2	13.58	0.220
16.86		0.737	183.6	15.28	0.249
19.86		0.868	242.3	27.2	0.279
21.48		0.939	292.2	52.9	0.311
22.87		1.000	512.2		0.512

Table 8. Desorption isotherm data, first cycle

p mm Hg	p_o mm Hg	p/p_o	q, $\frac{gm}{gm} \times 10^3$	$\frac{p}{q(p_o-p)}$
22.12	22.87	0.967	430.5	68.5
21.72		0.950	376.0	50.2
21.35		0.934	329.2	42.7
18.94		0.828	270.6	17.81
17.35		0.759	242.4	12.97
14.01		0.613	195.4	8.09
13.01		0.569	158.6	8.32
9.32		0.408	124.6	5.52
6.98		0.305	109.4	4.02
4.26		0.186	73.34	3.12
2.44		0.107	42.51	2.81
1.18		0.052	19.35	2.81
0.27		0.012	12.26	0.97
0.30		0.013	11.76	1.13
0.27		0.012	11.64	1.03
0		0	10.90	0

Table 9. Adsorption isotherm data, second cycle

mm Hg	mm Hg	p/p_o	q, $\frac{gm}{gm} \times 10^3$	$\frac{p^a}{q(p_o-p)}$	$\frac{q^a}{p/p_o}$
0.08	22.87	0.003	12.12	2.83	0.413
0.34		0.015	13.68	5.43	0.185
1.24		0.054	17.11	9.23	0.115
1.53		0.067	18.44	9.51	0.113
2.60		0.114	22.18	11.37	0.099
3.64		0.159	26.22	12.36	0.096
4.11		0.180	27.58	13.13	0.093
4.32		0.189	28.50	13.23	0.093
4.79		0.209	30.55	13.48	0.094
5.37		0.235	33.34	13.67	0.095
6.01		0.263	39.21	12.59	0.108
6.35		0.278	42.22	12.27	0.113
6.80		0.297	46.73	11.81	0.121
7.06		0.309	49.21	11.66	0.124
7.42		0.324	54.06	11.13	0.133
7.84		0.343	57.97	11.08	0.137
8.56		0.374	66.14	10.83	0.148
9.02		0.394	71.09	10.82	0.153
9.62		0.421	77.69	10.87	0.159
10.76		0.470	87.77	11.56	0.164
12.41		0.543	107.1	12.33	0.177
14.32		0.626	139.1	13.06	0.205
15.79		0.690	175.3	13.56	0.238
17.16		0.750	200.9	15.82	0.253
18.38		0.804	222.3	19.36	0.263
19.42		0.849	241.4	24.42	0.271
20.27		0.886	256.5	31.7	0.277
20.85		0.912	275.8	39.0	0.290
21.43		0.937	294.8	52.4	0.303
22.87		1.000	697.9		0.698

[a]Based on isotherm beginning at q equal to zero.

Table 10. Desorption isotherm data, second cycle

mm Hg	mm Hg	p/p_o	q, $\frac{gm}{gm} \times 10^3$	$\frac{p^a}{q(p_o-p)}$
22.52	22.87	0.985	462.0	142.6
22.18		0.970	412.7	80.0
21.67		0.948	349.2	53.4
21.21		0.927	315.1	42.0
20.12		0.880	279.7	27.2
18.27		0.799	248.5	16.72
17.17		0.751	231.0	13.69
15.32		0.670	204.3	10.49
14.54		0.636	188.5	9.83
13.92		0.609	170.7	9.73
12.90		0.564	152.6	9.13
11.37		0.497	133.1	8.09
9.67		0.423	119.9	6.72
7.05		0.308	103.4	4.82
5.64		0.247	90.46	4.11
6.14		0.268	87.66	4.78
6.07		0.265	87.66	4.71
6.06		0.265	87.66	4.70
5.32		0.233	81.06	4.32
3.80		0.166	58.35	4.20
2.77		0.121	36.82	5.32
1.80		0.079	6.37	-1.89
0.09		0.004	-0.62	-0.34
0.02		0.001	-1.57	

[a]Based on isotherm beginning at q equal to zero.

Table 11. Adsorption isotherm data, third cycle

p mm Hg	p_o mm Hg	p/p_o	q, $\frac{gm}{gm} \times 10^3$	$\frac{p}{q(p_o-p)}$	$\frac{q}{p/p_o}$
0.38	22.87	0.017	2.91	5.80	0.171
1.06		0.046	5.39	9.02	0.117
1.70		0.074	8.73	9.20	0.118
2.95		0.129	13.52	10.95	0.105
3.83		0.168	16.98	11.85	0.101
5.33		0.233	25.45	11.94	0.109
6.28		0.275	34.26	11.05	0.125
7.33		0.320	45.95	10.27	0.144
8.61		0.376	60.24	10.02	0.160
9.61		0.420	70.01	10.35	0.167
11.14		0.487	86.89	10.93	0.178
12.61		0.551	101.7	12.08	0.185
14.27		0.624	129.5	12.81	0.208
15.62		0.683	165.7	13.00	0.243
17.47		0.764	202.1	16.01	0.265
19.05		0.833	228.2	21.85	0.274
20.33		0.889	256.3	31.2	0.288
21.53		0.941	299.0	53.7	0.318
22.87		1.000	714.2		0.714

Table 12. Desorption isotherm data, third cycle

p mm Hg	p_o mm Hg	p/p_o	q, $\frac{gm}{gm} \times 10^3$	$\frac{p}{q(p_o-p)}$
22.50	22.87	0.984	446.1	136
22.21		0.971	416.7	80.8
21.94		0.959	384.2	61.4
21.66		0.947	345.8	51.8
21.36		0.934	324.1	43.6
20.66		0.903	296.9	31.5
19.93		0.871	279.3	24.27
18.19		0.795	249.2	15.60
16.46		0.720	226.6	11.33
15.21		0.665	206.5	9.62
14.45		0.632	191.9	8.94
13.43		0.587	171.9	8.28
12.64		0.553	155.8	7.93
11.66		0.510	139.8	7.44
9.85		0.431	125.5	6.03
7.08		0.310	108.6	4.13
5.78		0.253	94.8	3.57
3.29		0.144	55.15	3.05
1.19		0.052	17.49	3.14
0.28		0.012	9.99	1.24

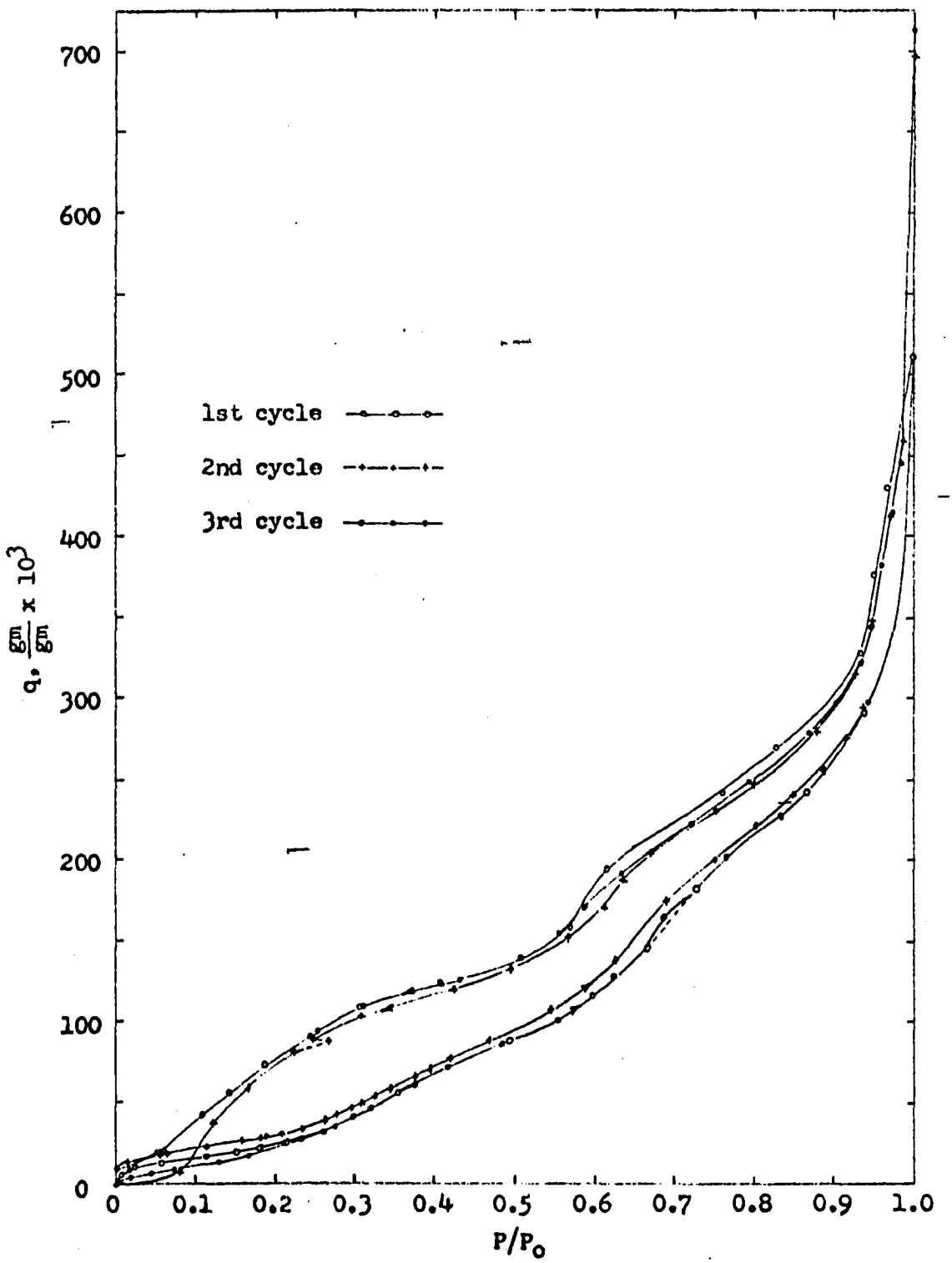

Figure 11. Adsorption and desorption isotherms of sodium montmorillonite

than was the adsorption branch. Johansen and Dunning (36) suggest the lack of reproducibility of adsorption is due to inability to desorb back to the beginning of the hysteresis loop which is very near zero relative pressure. The reason for this inability is discussed later in this report.

The data of the present study show that the adsorption branch is more closely reproduced on successive runs than is the desorption branch. After a p/p_o value of about 0.28, the adsorption curves for the first and third cycles follow one another very closely, within the experimental error discussed previously. The desorption curves for these two cycles are not in very good agreement until relative pressures below 0.30 are reached. Neither the adsorption nor desorption branches for the second run, which began at a higher value of q, agree very well with those for the other cycles. If the isotherms for the second cycle are started at the origin the agreement is much better for adsorption than for desorption. The data suggest that the adsorption, rather than desorption, branch may be the true equilibrium curve. This would be in agreement with the "ink bottle" theory of McBain (45) and the "open pore" theory of Foster (25), both of which explain the hysteresis on the basis of the shape and arrangement of the pores in which capillary condensation takes place. Since effective degassing can minimize the Zigsmondy type of hysteresis, the pore structure would probably be the main cause of hysteresis.

Barrer and MacLeod (5) studied the adsorption of various

non-polar and polar gases and vapors, including water vapor, by a sodium-rich montmorillonite. They explain the hysteresis observed when polar gases and vapors are adsorbed in the interlayer regions. If nucleation of an adsorbate-rich phase occurs around the periphery of crystallites poor in adsorbate, it must be associated with strain and interfacial free energies. These are positive and so slow down the free development of the adsorbate-rich phase until the pressure has exceeded the value for true thermodynamic equilibrium between the vapor and separated montmorillonite layers with and without interlayer adsorbate. On desorption the development of the adsorbate-poor phase in the interlayer region is delayed by strain and interfacial free energy until the pressure has fallen below that for true equilibrium. This results in a hysteresis loop. Barrer and MacLeod found the hysteresis observed on sorption of water vapor to be a composite loop associated with both capillary condensation and interlayer water.

Hirst (33) also developed an explanation for hysteresis associated with interlayer adsorption. Attractive forces between layers prevent penetration of the adsorbate until a threshold pressure is reached. These forces are then overcome by forces leading to penetration and the layers separate to admit a layer of adsorbate. The interlayer attraction is reduced by the expansion, so further separation requires less energy. However, the energy of adsorption is also less and a

second layer of adsorbate does not enter until a higher pressure is reached. On desorption the layers are initially separated and their attractive interaction weakened while the forces tending to separate them are high. The layers can not come together until the amount of interlayer adsorbate, and thus swelling pressure, are substantially reduced. Therefore, a hysteresis loop is observed.

According to Brunauer (13, p. 409) the adsorption process most probably causes a change in the pore volume which may be either reversible or irreversible. The pore volume change may result in different pore shapes and arrangements in the external surfaces of the montmorillonite sample. This may account for the difference in the adsorption curves prior to a relative pressure of about 0.28 for the first and third cycles. X-ray diffraction data, the initial adsorption curve of Figure 7, shows that at a p/p_o of about 0.20 the uptake of water into the interlayer regions begins and that at p/p_o about 0.28 the rate of increase in interlayer spacing with p/p_o reaches a maximum and nearly constant value. It is in this region that the adsorption curves begin their agreement, suggesting that the effect of the interlayer surfaces far outweighs that of the external surfaces.

The general shape of the adsorption and desorption isotherms in Figure 11 is very similar to those presented elsewhere (5,20,36,51). The adsorption curve displays a rather steep portion between relative pressures of 0.25 to

0.45 followed by a somewhat less steep portion. Another steeper portion begins at a relative pressure around 0.65. Demirel (20) observed similar behavior in the p/p_o range of 0.65 to 0.75. On the basis of X-ray data from Mooney et al. (52), Hendricks et al. (32) and his own, he deduced that the behavior occurred when the layer separations approached the thickness of two water molecules. However, the present study, Figure 7, shows that it corresponds to the region in which the second increment of layer separation (or uptake of a second layer of interlayer water) begins to take place.

Figure 7 alwo shows that the steeper portion between p/p_o of 0.25 to 0.45 on Figure 11 corresponds to the first increment of layer separation. The argument proposed by Barrer and MacLeod (5) explains the form of the adsorption isotherm of this study. The initial water adsorbed is mainly confined to the external surfaces of the clay. After an approximate threshold pressure is reached the water molecules penetrate more freely between clay sheets and cause separation. With water vapor, a second stage of interlayer adsorption occurs and is reflected by the second steeper portion of the adsorption isotherm. As p/p_o approaches 1.0, capillary condensation is added to the interlayer adsorption. The X-ray data, Figure 7, show that a third increment of layer separation also occurs at high relative pressures.

The desorption isotherms show a pronounced dip in the relative pressure range from about 0.65 to 0.30. This is also

shown in data of other investigators (5,36,51).. Demirel's data (20) for sodium montmorillonite give no experimental points in this range, but his calcium montmorillonite displayed a very similar dip in the p/p_o range of 0.30 to less than 0.10. Barrer and MacLeod (5) attribute the steep portion of this dip to the removal of interlayer adsorbate; the process occurring at an approximate threshold pressure below that for the adsorption curve. The X-ray data of Mooney et al. (52) would tend to support this; however, as was discussed earlier, their data probably does not include the final increment of layer separation and so may not be representative of the actual case. The data of the present study (desorption curve of Figure 7) show that the basal spacing remains nearly constant at 16 Å in the relative pressure range 0.65 to 0.50 corresponding to the steep portion of the desorption isotherm. This would indicate that the greater portion of the water being desorbed is from the external surfaces of the sample.

Barrer and MacLeod (5) also observed a hysteresis loop for the adsorption-desorption of non-polar gases and vapors on their montmorillonite. Since the non-polar adsorbates were adsorbed only on the external surfaces, the reasons extended for hysteresis with polar adsorbates are not applicable. They suggest that when the clay is lubricated by a film of capillary condensate some of the clay particles are drawn by surface tension forces into a thixotropic structure. This more regular array then retains capillary condensed adsorbate

more firmly than would a purely random array. When the film of capillary condensate becomes sufficiently dilute it ceases to lubricate and hold the thixotropic structure together. The array then becomes more random again and must give up the remaining condensate. The desorption isotherm becomes steeper when this occurs and, with non-polar adsorbates, closes the hysteresis loop.

In view of the X-ray data obtained in the present study, it is proposed that the above argument may be applied to the desorption of water vapor in the relative pressure range of 0.65 to 0.50. The steep portion of the desorption isotherm in this range is, therefore, due to the destruction of a thixotropic structure with its accompanying release of capillary condensed water. The second layer of interlayer water is withdrawn in the p/p_o range of 0.50 to about 0.30, which corresponds to a flatter portion of the isotherm. At a p/p_o of about 0.30 another steep portion begins. The x-ray data, Figure 7, show that this corresponds with the beginning of removal of the last layer of interlayer water. The hysteresis explanation of Hirst (33) and that of Barrer and MacLeod (5) for polar adsorbates are applicable in this region.

A possible explanation for the more complete desorption for the second cycle than for the first and third cycles of this study is proposed. Figure 11 shows a break in the second desorption curve at a relative pressure of about 0.25. After reaching this point no vapor transfers were made for a period

of eighteen days. At the end of this period it was observed that the sample had desorbed more water and the relative pressure had increased, as shown by the shift (dashed line) to a point lower and to the right. Two more days disclosed no additional change in position. The next vapor transfer caused a shift down and to the left (second dashed line) in one day. Before the eighteen day period of no vapor transfers, it had appeared that the second desorption curve was approaching the path followed in the first run and which was later followed in the third cycle. However, after the idle period the desorption curve became steeper and the zero value of q was attained with relative ease. On the third run, with no prolonged non-vapor-transfer period, a special effort was made to reach the initial value of q. Even with a final pumping period extending over a period of three weeks the value of q could not be brought substantially lower than that attained on the first run. This suggests that the remaining water was trapped in external pores (such as McBain's "ink bottle" pores) and/or the interlayer regions. X-ray diffraction data, Figure 7, indicate that at a relative pressure of 0.25 the last layer of interlayer water has started to be withdrawn; this is also shown by the data of Mooney et al. (52) and of Gillery (27) reproduced in Figure 9. The prolonged period of no vapor transfers may allow for particle rearrangement and for escape of water from pores and interlayer regions which would be blocked off by contraction of the mass on further desorption.

Figure 12 is a highly idealized schematic diagram of the possible mechanism of entrapping water in the adsorbent. Takizawa (59), in a study of water vapor adsorption on Niigata Bentonite, found similar quantities of residual water left on completion of desorption. He attributed the retained water at zero pressure mainly to hydration of the cation. His desorption readings were taken at 24 to 48 hour intervals, so insufficient time would be available for the escape of trapped water as suggested above.

The behavior discussed above for a prolonged non-vapor-transfer period would indicate that equilibrium was not attained in the 24 hour period between vapor transfers, at least in that region of the desorption isotherm. However, in an earlier incomplete study with the same sodium montmorillonite material there was a similar non-vapor-transfer period of twenty days at a relative pressure of about 0.69 on the desorption curve. At the end of the twenty day period there was no significant change in the location of the point observed one day after the vapor transfer, indicating that equilibrium was very nearly attained in the 24 hour period. The X-ray data of Figure 7 show that the average basal spacing remains very nearly constant at about 16 Å in the relative pressure region 0.70 to 0.55 on the desorption curve, indicating that interlayer water may be held quite strongly in this region. The data of Mooney et al. (52) show that the basal spacing begins to decrease at a p/p_o of 0.70. However, as

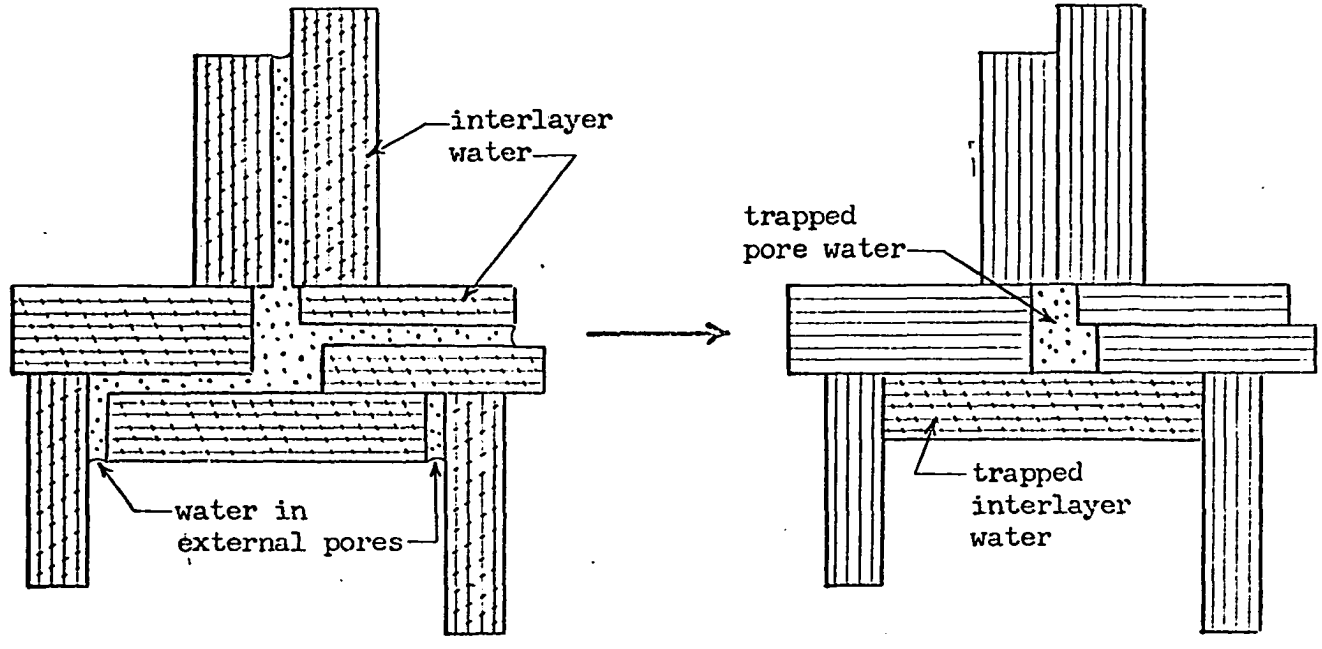

Figure 12. Idealized schematic diagram of possible mechanism of water entrapment

discussed before, their desorption curve may be shifted because of incomplete saturation.

No relaxation of the type described here was observed for adsorption runs; 24 hours were enough for attainment of equilibrium.

BET Parameters

The values of the BET function, $\frac{p}{q(p_o-p)}$, tabulated in Tables 7, 8, 9, 10, 11 and 12 are plotted against the relative pressure, p/p_o, in Figures 13, 14 and 15 for the first, second and third sorption cycles, respectively.

Generally, BET plots will have a straight line region only between p/p_o values of 0.05 to about 0.3 (1, p. 481). Each of the Figures 13, 14 and 15 shows that a fairly straight line is obtained with adsorption data in the p/p_o range of 0.05 to about 0.18. Comparison with the initial adsorption curve for basal spacings in Figure 7 reveals that at a p/p_o of 0.18 the first increment of interlayer separation is just beginning. The line width data of Figure 7 suggests that some uptake of interlayer water occurs at low relative pressures; however, the constant basal spacing indicates that most of the water is adsorbed on the external surfaces of the clay in the p/p_o range below 0.18. On this basis it was concluded that the linear BET plot represents adsorption taking place predominantly on the external surfaces, and the BET parameters q_m and C obtainable from the linear BET plot represent the

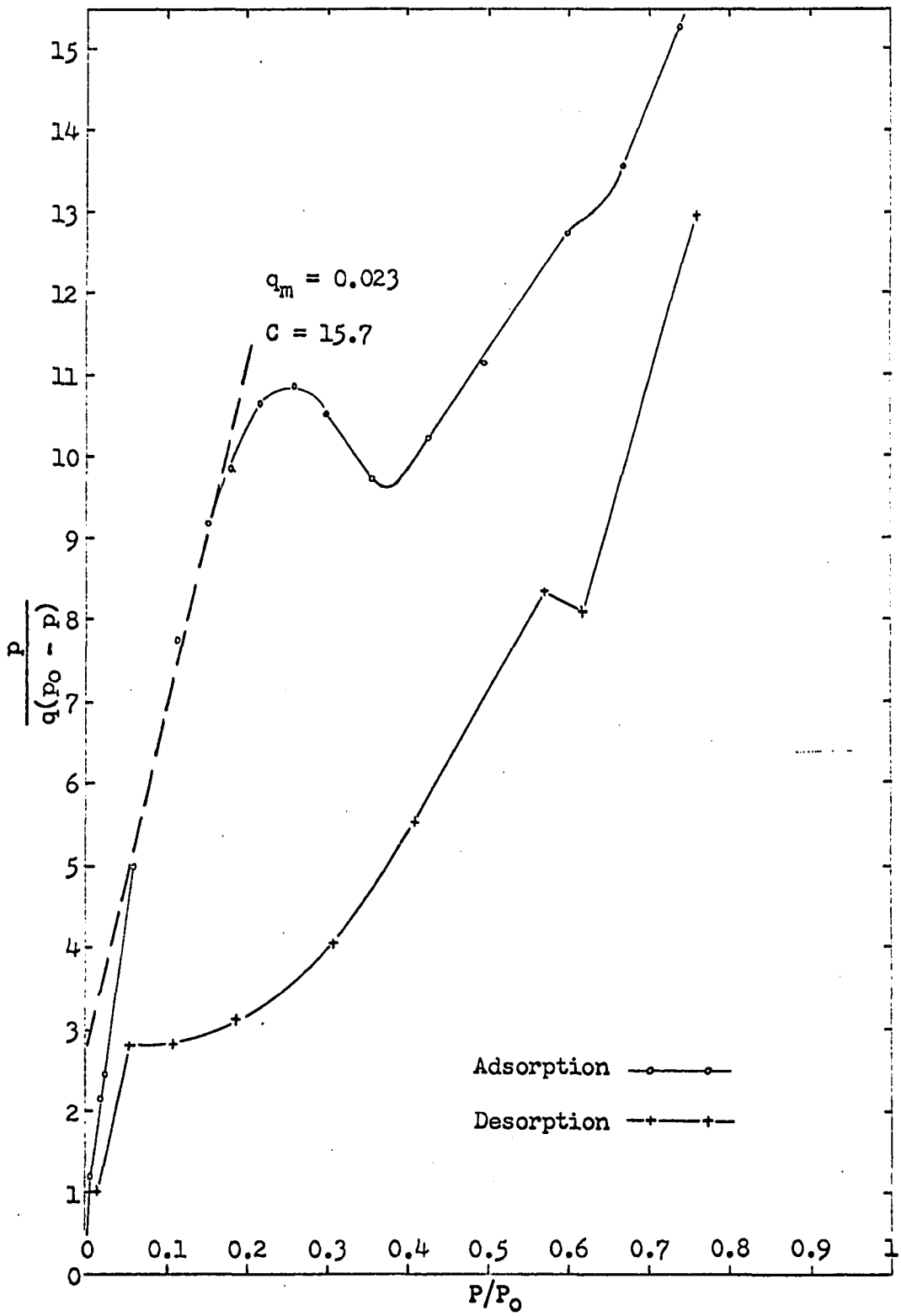

Figure 13. BET plot of sorption data for water vapor on sodium montmorillonite, first cycle

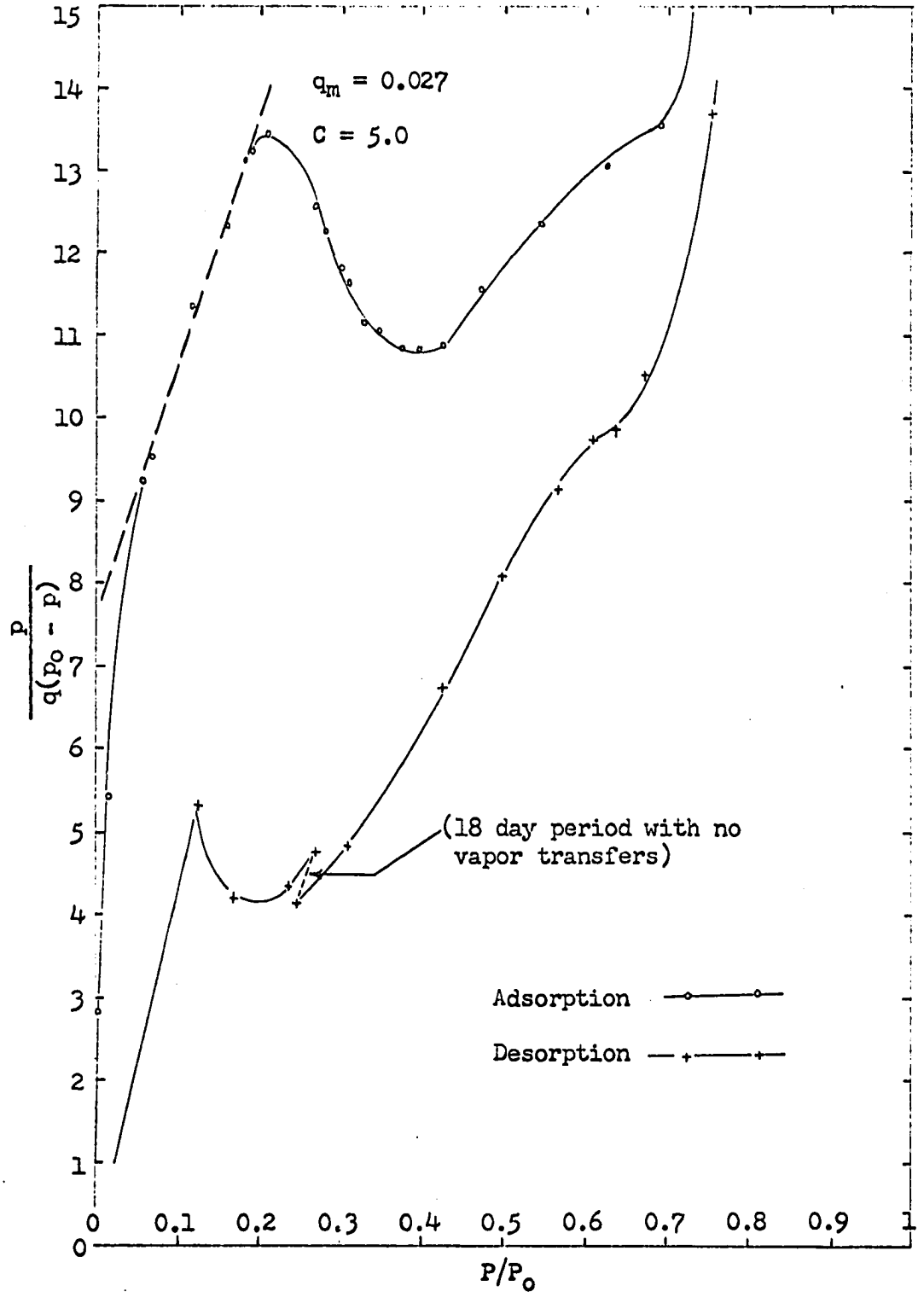

Figure 14. BET plot of sorption data for water vapor on sodium montmorillonite, second cycle

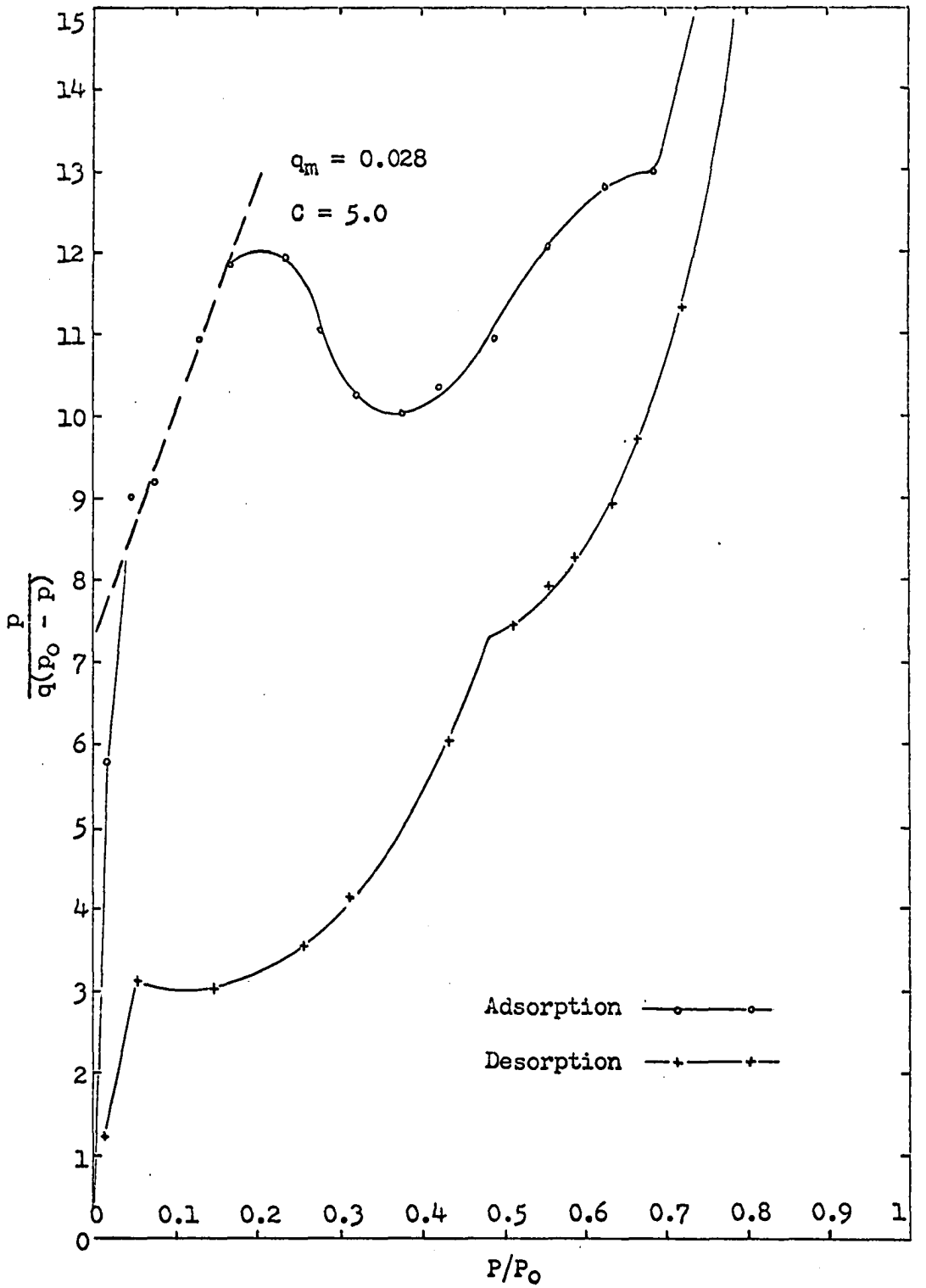

Figure 15. BET plot of sorption data for water vapor on sodium montmorillonite, third cycle

external surfaces of the sodium montmorillonite. The heavy dashed straight lines on the BET plots were fitted from the experimental data by the method of least squares and the parameters q_m and C determined by Equation 4b. The values obtained are given on the figures.

The BET plots show that the function $\frac{p}{q(p_o-p)}$ reaches a relative maximum at a p/p_o of about 0.20 to 0.25, then decreases to a relative minimum at a p/p_o of about 0.40 before climbing again. Bartell and Dobay (7) report a similar behavior, at higher relative pressures, for the adsorption of aliphatic amine vapors on silica gel; they concluded this behavior defied physical interpretation. The X-ray data of the present study shows that the negative slope of the BET function corresponds with the initial portion of the first increment of interlayer expansion. Further comparison of Figure 7 with the BET plots reveals that an inflection point on the BET plot between p/p_o values of 0.60 and 0.70 corresponds with the completion of the first molecular layer of interlayer water and the beginning of the second increment of expansion. The present data suggest the behavior observed by Bartell and Dobay may have been caused by an expansion or particle rearrangement which made accessible areas of the adsorbent surface not initially available for adsorption.

The relative pressure range from about 0.2 to 0.7, during which adsorption takes place on all surfaces of the sodium montmorillonite, is not in the BET relative pressure range

(0.05 to 0.3) in which the BET plot is expected to be linear. Demirel (20), comparing the data for sodium and calcium montmorillonites, attempted to extrapolate the second part of the BET plot for sodium montmorillonite to low pressures, producing a straight line in the BET range, in order to obtain estimates of the parameters q_m and C for all surfaces. The more extensive data of the present study shows that the location of his extrapolated straight line is not definite. The present data show a somewhat linear BET plot between relative pressures of 0.4 to 0.6 which is outside the usual BET range. The 0.4 to 0.6 relative pressure range represents adsorption on both external and internal surfaces, a monomolecular layer of water being completed in the interlayer region at a p/p_o of about 0.6. If this portion of the BET plots is extrapolated back to zero pressure, the values of q_m obtained are 0.054, 0.058 and 0.055 and the values of C are 4.5, 2.6 and 3.6 for the first, second and third cycles, respectively, as compared to a q_m of 0.078 and a C of 1.4 obtained by Demirel. The validity of using the parameters so obtained in the present study for determination of surface areas, or of the area occupied per water molecule on the sodium montmorillonite surface, is questionable since the amount of adsorption on the external surfaces is not known.

The BET plots for desorption data are included in Figures 13, 14 and 15 since desorption data has been suggested and used by others (36,51,52) for evaluation of the BET parameters.

A somewhat linear portion of the plots can be observed in the relative pressure range 0.3 to 0.5 which is above the usual BET range. Mooney et al. (51) observed a linear BET desorption plot, in the usual BET range, for sodium montmorillonite (Volclay-SPV) but in a later study (52) obtained a BET plot very similar to those of the present study. The X-ray data of this study, Figure 7, shows that in the p/p_o range of 0.5 to 0.3 the second molecular layer of interlayer water is being removed.

External surface areas

The values of q_m obtained from the three adsorption BET plots are given on Figures 13, 14 and 15. If the area of the adsorbent surface occupied by each water molecule of the monolayer were known, the external surface area per gram of sodium montmorillonite could be calculated by Equation 7. If the molecules are in a closest packing arrangement, Equation 8 yields a value of 10.8 $\mathring{A}^2$ per water molecule. However, as discussed earlier (pp. 52-55), several investigators (6,20,23, 24,31,42) have suggested other spatial geometric arrangements for the water molecules on the clay surface which result in other than closest packing for the monolayer coverage. The arrangement proposed by Hendricks and Jefferson (31) gives an area of about 11.5 $\mathring{A}^2$ per water molecule; the basal plane of ice structures proposed by Macey (42), Demirel (20) and Forslind (23) give an area of about 17.5 $\mathring{A}^2$; the arrangements

proposed by Barshad (6) yield values of about 11.5 $Å^2$ and 7.7 $Å^2$, depending on the arrangement at the clay surface. External surface areas per gram of sodium montmorillonite, A_e, were computed by Equation 7 utilizing each of the water molecular areas, s, given above and the values of q_m obtained from the adsorption data. The results are given in Table 13. It can

Table 13. External surface areas per gram of sodium montmorillonite calculated from water vapor adsorption data

Cross-sectional area per water molecule, A^2	External surface area, A_e, m^2/gm		
	First cycle $q_m = 0.023$	Second cycle $q_m = 0.027$	Third cycle $q_m = 0.028$
10.8[a]	83.0	97.4	101.1
11.5[b]	88.3	103.7	107.5
17.5[c]	134.4	157.8	163.7
7.7[d]	59.2	69.4	72.0

[a]Based on closest packing.

[b]Based on arrangements of Hendricks and Jefferson (31) and Barshad (6).

[c]Based on ice structure (20).

[d]Based on arrangement of Barshad (6).

be observed that the external surface area increased with successive adsorption-desorption cycles, the values for the second and third cycles being very close together. As

mentioned in the discussion of the sorption iostherms, the adsorption-desorption process may result in different pore shapes and volumes in the external surfaces and in different arrangements of the external surfaces, thus making more area available for adsorption. The values obtained are larger than those reported by others as determined from nitrogen adsorption, i.e. 41 to 71 m^2/gm by Emmett et al. (22), 33 m^2/gm by Mooney et al. (51), 38 m^2/gm by Johansen and Dunning (36) and 34.5 m^2/gm by Zettlemoyer et al. (63). This indicates that some portions of the external surfaces are accessible to water vapor but not to nitrogen. Also, as the line width data of Figure 7 shows, there may be a small amount of water penetration into interlayer regions.

Heat of adsorption

The BET parameters C were used to calculate the average heat of adsorption, less the heat of liquefaction, of the first adsorbed monomolecular layer of water by using Equation 5 to obtain:

$$E_1 - E_L = RT\ln C = (1.987)(297.5)\ln C \quad \text{cal/mole}$$

The values obtained were corrected according to Clampitt and German (17) by using their correction value (see p. 8) to obtain:

$$E_1 - E_L = RT\ln C + (\Delta H_s - E_L)$$
$$= (1.987)(297.5)\ln C + 1700 \quad \text{cal/mole}$$

The corrected and uncorrected values are listed in Table 14 for several sodium montmorillonites for which water vapor adsorption data is available. The values show reasonably good agreement with one another. Zettlemoyer et al. (63) used calorimetric techniques in heat of immersion studies with a natural Wyoming bentonite (predominantly sodium montmorillonite) and found the difference between the heat of immersion for the clean surface and that for a monolayer of water on the external surfaces to be 575 ergs/cm^2, the external surface area being 34.5 m^2/gm as determined by their nitrogen adsorption data. This gives a value of 19.84 joules (or 4.74 calories) per gram of montmorillonite. The present study shows that the amount of water adsorbed, q_m, when the external surfaces are covered by a monolayer of water is from 0.023 to 0.028 grams per gram of sodium montmorillonite. Using these data, we obtain $(E_1 - E_L)$ values of 3.0 to 3.7 Kcal/mole, which are of the same order of magnitude as the corrected $(E_1 - E_L)$ values listed in Table 14. This comparison shows the reasonableness of the parameter C in the BET equation.

Zettlemoyer et al. used their heat of immersion and adsorption isotherm data to determine heats of desorption (or adsorption) of water from bentonite at 25° C (63, Figure 4). The curve presented does not show good agreement with the isosteric heat of desorption curve for sodium montmorillonite (Wyoming) obtained by Mooney et al. from desorption isotherm data (51, Figure 5). However, the curve of Zettlemoyer et al.

Table 14. BET parameters and average heat of adsorption of a monomolecular layer of adsorbed water, calculated from water vapor adsorption data for sodium montmorillonites

Source of data and material	BET parameters		Average heat of adsorption less heat of liquefaction, $E_1 - E_L$, Kcal/mole	
	q_m	C	According to Brunauer (13)	Corrected according to Clampitt and German (17)
Orchiston (55)				
Arizona montmorillonite	0.093	5.9	1.1	2.8
Hendricks et al. (32)[a]				
California montmorillonite	0.091	8	1.2	2.9
Mississippi montmorillonite	0.070	8	1.2	2.9
Wyoming montmorillonite (Volclay)	0.023	13	1.5	3.2
Johansen and Dunning (36)				
Wyoming montmorillonite (Volclay)	0.056	--	--	--
Demirel (20)				
Wyoming montmorillonite (Volclay-SPV)	0.021	9	1.3	3.0
Roderick (present study)				
Wyoming montmorillonite (Volclay-SPV)				
first cycle	0.023	15.7	1.6	3.3
second cycle	0.027	5.0	1.0	2.7
third cycle	0.028	5.0	1.0	2.7

[a]BET parameters calculated by Demirel (20, Figures 23 and 25).

shows quite good agreement with the isosteric heat of adsorption data obtained by Takizawa (59) from water vapor adsorption isotherms with Niigata bentonite. This may indicate that the adsorption isotherm is nearer the true equilibrium curve than is the desorption isotherm.

Comparison of BET parameters from other data

It is interesting to compare the BET parameters obtained in the present study with those reported by other investigators for the adsorption of water vapor on sodium montmorillonites. The values of the parameters reported are tabulated in Table 14. Demirel (20) used the same material as that used for this study. The values of q_m listed for his data and for Hendricks et al. sodium saturated Wyoming montmorillonite are close to those of the present study, especially for that of the first cycle. BET plots for the data of Demirel and of Hendricks et al., presented by Demirel (20, Figures 20 and 25), show the characteristic hump at a relative pressure of about 0.20 illustrated in Figures 13, 14 and 15 of this study. Among the sodium montmorillonites for which data are available, this behavior of the BET function appears to occur only with the Wyoming montmorillonite (Volclay). Demirel's plots for Hendricks et al. California and Mississippi sodium saturated montmorillonites (20, Figures 23 and 25) do not show such a hump. The value of q_m obtained from Johansen and Dunning's (36) data for Wyoming montmorillonite (Volclay) would seem to

be an exception; however, their data (36, Figure 2) show that there were no experimental observations in the p/p_o range in which the hump occurred in the BET plots from data for other Wyoming montmorillonite samples. It is also noted that the q_m value of 0.056 obtained with their data is in very good agreement with the values of 0.054, 0.058 and 0.055 obtained by extrapolating the nearly linear portions of the present BET plots in the p/p_o range of 0.4 to 0.6 back to zero pressure. Mooney et al. (51) also used Wyoming montmorillonite (Volclay) but did not give their adsorption data; their adsorption isotherm plot does not give enough experimental observations to permit calculation of BET parameters.

The q_m values for Orchiston's Arizona montmorillonite and Hendricks et al. California montmorillonite are in good agreement. The BET data for Orchiston's material display an interesting feature. At a p/p_o of 0.05 his data give a BET function, $\frac{p}{q(p_o-p)}$, value of 4.39; this drops to 2.65 at a p/p_o of 0.10 and then climbs in the linear path he used to determine the BET parameters. Demirel observed a similar behavior with his calcium montmorillonite (20, Figure 21), but at lower pressures, the high point being at a p/p_o of 0.013. These observations are below the usual BET range and the discrepancies may be due to the decreased accuracy of pressure and mass increase determinations at low pressures. However, the X-ray data of Mooney et al. (52) and Demirel (20) for calcium montmorillonite show that interlayer expansion occurs at very

low pressures. Therefore, the high point on the BET plot may represent a behavior similar to that observed much more clearly with the present data, i.e. adsorption on external surfaces before penetration of the water between clay layers. If this interpretation is applied to Orchiston's data it would suggest that for water vapor adsorption on the sodium Arizona montmorillonite interlayer expansion would begin at a relative pressure near 0.05, appreciably below that observed with sodium Wyoming montmorillonite. This again illustrates the effect of the source of material on the X-ray basal spacing data obtained and accounts, in part, for the wide scatter of observed X-ray data for sodium montmorillonites discussed earlier.

Free Energy Changes

The values of the function $\frac{q}{p/p_o}$ tabulated in Tables 7, 8, 9, 10, 11 and 12 are plotted against p/p_o for each of the three adsorption runs in Figure 16. Van Olphen (61) has used such plots, based on the desorption data of Mooney et al. (51,52), to obtain estimates of short range repulsion energies between clay layers. Demirel (20) used similar plots to determine free energies of wetting of sodium and calcium montmorillonites.

The general shape of the $\frac{q}{p/p_o}$ versus p/p_o plots are the same for the three runs; some variations can be observed. The reasons for the variations are the same as those discussed

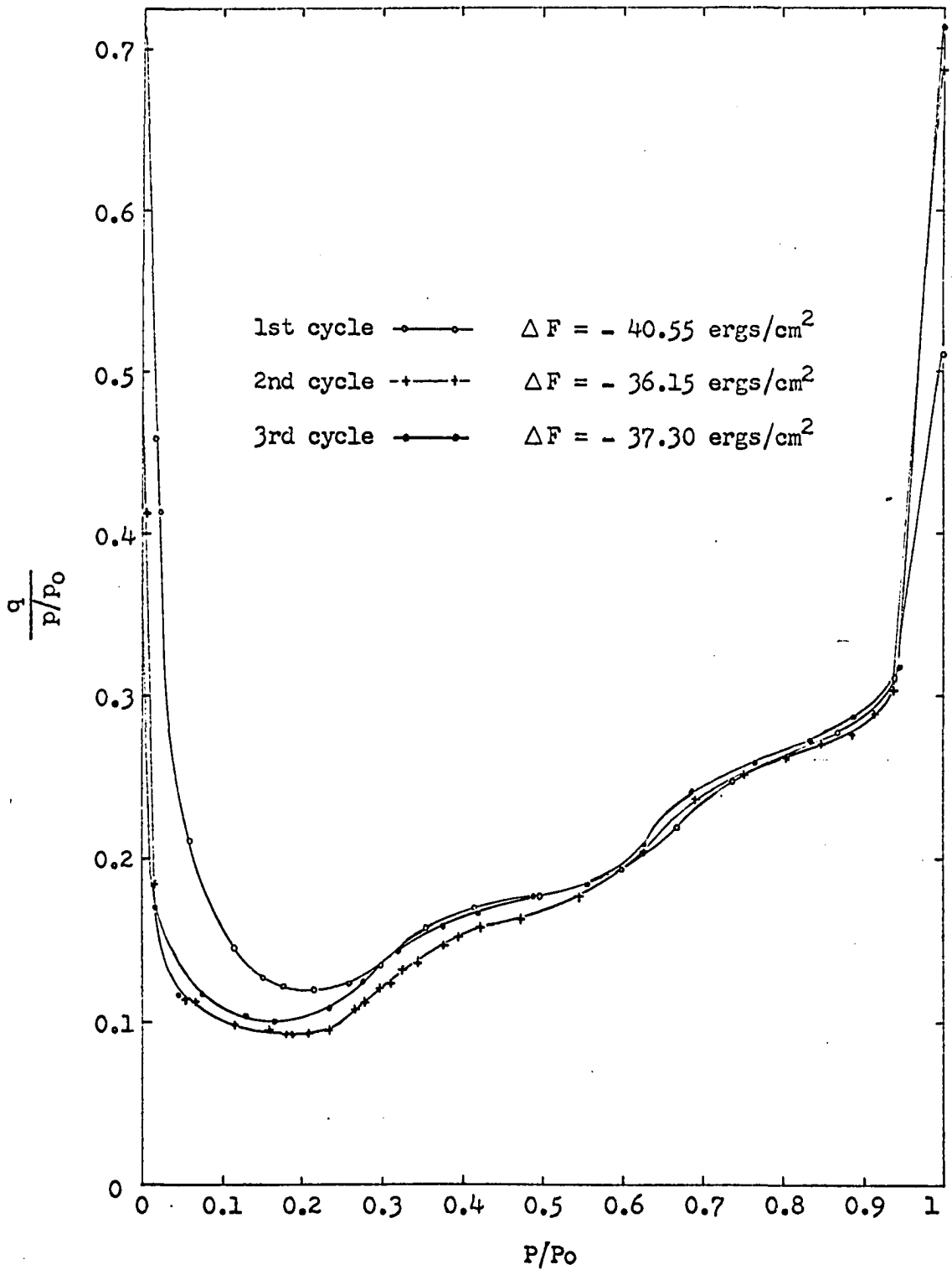

Figure 16. Plots for graphical integration of Equation 2 for water vapor adsorption on sodium montmorillonite

earlier for the differences observed in the adsorption isotherms (p. 73).

Free energy of wetting

The free energies of wetting as defined by Equation 3a were calculated by using Equation 2 (p. 3). The numerical values of the integral in Equation 2 were determined by graphical integration of the curves presented in Figure 16. Integration was accomplished both by measuring the areas beneath the curves and by weighing with an analytical balance. The values obtained by the two methods were within one percent of one another. The values of the integrals thus found were 0.2210, 0.1970 and 0.2052 gm/gm for the first, second and third runs, respectively. From the limits of experimental errors discussed earlier, the error in these values were estimated to be about ±6%.

The specific surface term, Σ, of Equation 2 was determined from crystallographic data for sodium montmorillonite by the relationship:

$$\Sigma = \frac{N\sigma}{M_s}$$

where N is Avogadro's constant, M_s is the formula $(Al_{3.34}Mg_{0.06}Si_8O_{20}(OH)_4Na_{0.66})$ weight of a unit cell layer and σ is the area exposed by one unit cell layer. M_s is equal to 742 and σ is equal to 2 x 5.16 x 8.94 $Å^2$, where 5.16 Å and 8.94 Å are the unit cell dimensions a_o and b_o, respectively

(20). Substituting these values in the above expression, a specific area, Σ , of 748 m^2/gm of sodium montmorillonite is obtained. Substituting this value into Equation 2, the free energies of wetting were calculated by:

$$\Delta F = -\frac{RT}{M} I$$

$$= -\frac{(8.314 \times 10^7)(297.5)}{(18.02)(748 \times 10^4)} I$$

where I is the value of the integrals determined by graphical integration as discussed above. The free energies of wetting thus determined were -40.55 ± 2.43, -36.15 ± 2.17 and -37.30 ± 2.24 $ergs/cm^2$ for the first, second and third adsorption runs, respectively. These values are in good agreement with that of -34.76 ± 1.91 $ergs/cm^2$ determined by Demirel (20) for sodium montmorillonite. Although data were scarce at high and low pressures for the desorption data of Mooney et al., van Olphen (61) estimated a total energy change of somewhat more than 100 $ergs/cm^2$ for sodium montmorillonite.

By Equation 3a, the values determined for the free energies of wetting are equal to:

$$\Delta F = (\gamma_{sl} - \gamma_{so}) + \alpha\Delta V \quad ergs/cm^2 \text{ average surface}$$

for sodium montmorillonite. If the area of the surface occupied by a water molecule were known the external surface area determined by the BET method for water vapor adsorption could be used to evaluate α, the interstitial surface area

per cm^2 of total surface. However, this would still leave two unknowns, $(\gamma_{sl} - \gamma_{so})$ and ΔV, so the equation could not be solved unless one of the unknowns could be found independently or another independent relationship between them was determined. The rather large error in determination of α by the BET method would seem to rule out solution of the two unknowns by simultaneous equations corresponding to different values of α for the same material as suggested earlier by Demirel (20).

Free energy changes on adsorption

Fu and Bartell (26), in their paper on the surface area of porous adsorbents, evaluated the integral $\frac{RT}{M}\int_0^{p/p_o} \frac{q}{p/p_o} d(p/p_o)$ at various values of p/p_o for the adsorption of vapors on porous solids. When q is the mass of vapor adsorbed per gram of solid, the value obtained is the free energy change, $A\Delta F$ in ergs/gm of solid, for adsorption from a relative pressure of zero to p/p_o. When the values of $A\Delta F$ were plotted against p/p_o a curve consisting of two portions was obtained; each portion could be represented by an equation of the form $A\Delta F = \alpha(p/p_o)^{\beta}$, where α and β are constants different for the two portions of the curve. If $\log(A\Delta F)$ was plotted against $\log(p/p_o)$, two straight line portions were obtained. From the intersection of the two portions of the curve and from the hypothetical process they proposed, Fu and Bartell (26) were

able to derive an expression for the specific surface of rigid porous adsorbents which did not involve assigning a molecular area to the adsorbate. They tested their method with a variety of adsorbents and adsorbates; the specific surfaces obtained were found to be in very good agreement with those determined by the BET nitrogen adsorption method.

In discussing their method, Fu and Bartell (26) state: "It is also conceivable that, with suitable interpretations, this method can be utilized to study the expansion or deformation of porous materials caused by the adsorption of various vapors." Sodium montmorillonite is a porous material which undergoes expansion with adsorption of water vapor; therefore, it was felt that an analysis similar to that of Fu and Bartell may be instructive. Therefore, the values of the integral $\int_0^{p/p_o} \frac{q}{p/p_o} d(p/p_o)$ for increasing increments of p/p_o, up to and including the saturation point, for the adsorption data of the present study were determined by graphical integration as discussed earlier. This was also done with Demirel's (20) adsorption data for sodium montmorillonite. Values of the integrals were thus obtained for four complete water vapor adsorption runs involving two separate samples of the material. These values were multiplied by $-\frac{RT}{m} = -\frac{(8.314 \times 10^7)(297.5)}{18.02}$ to obtain the free energy changes, $A\Delta F$ ergs/gm of sodium montmorillonite, due to adsorption to a relative pressure of

p/p_o. The values of $A\Delta F$ thus obtained are presented in Table 15.

Plots of $\log(A\Delta F)$ versus $\log(p/p_o)$ are presented in Figures 17, 18, 19 and 20 for each of the adsorption runs. Each of the plots display three straight line portions (implying equations of the type $A\Delta F = \alpha(p/p_o)^{\beta}$ for various portions) rather than the two obtained by Fu and Bartell. Above a p/p_o of about 0.05 a linear plot is obtained to a p/p_o of 0.16 to 0.18. There is then a transition to another linear portion which continues to a p/p_o of about 0.65. This is followed by another linear portion to a p/p_o of about 0.95; the value at saturation lies above the extension of this last straight line portion. The portions of the plots below p/p_o of about 0.05 are not strictly linear but breaks in the slopes of the plots can be observed in the p/p_o range from 0.045 to 0.055. This is in agreement with the observations of Fu and Bartell; they reported nonlinearity below relative pressures of 0.05 and attributed it to the decreased accuracy in determining q values at very low pressures (26). In their development they disregarded this portion of the plots since it was not required for the determination of the surface area of the adsorbents.

Comparison of Figures 17, 18, 19 and 20 with the X-ray data for the initial adsorption run presented in Figure 7 reveals several interesting correlations. It may be seen that the break in the $\log(A\Delta F)$ plot at a p/p_o of 0.16 to 0.18

Table 15. Free energy changes per gram of sodium montmorillonite due to adsorption of water vapor

p/p_o	Free energy change (-AΔF) ergs/gm			
	Sample No. 1 present study			Sample No. 2 Demirel's study
	1st run	2nd run	3rd run	
0.01	1.20×10^7	0.52×10^7	0.35×10^7	0.46×10^7
0.02	2.01	0.83	0.61	0.83
0.03	2.55	1.04	0.84	1.11
0.04	3.02	1.22	1.04	1.35
0.05	3.38	1.40	1.23	1.56
0.06	3.69	1.55	1.41	1.76
0.07	3.97	1.71	1.58	1.94
0.08	4.23	1.86	1.74	2.11
0.09	4.46	1.99	1.90	2.27
0.10	4.68	2.13	2.05	2.42
0.12	5.09	2.40	2.34	2.72
0.14	5.47	2.67	2.62	3.01
0.16	5.82	2.94	2.90	3.29
0.18	6.16	3.20	3.17	3.56
0.20	6.49	3.45	3.44	3.83
0.22	6.82	3.71	3.72	4.12
0.24	7.11	3.97	4.01	4.41
0.26	7.50	4.25	4.31	4.72
0.28	7.85	4.55	4.65	5.04
0.30	8.21	4.88	5.00	5.38
0.34	9.01	5.61	5.77	6.13
0.38	9.90	6.40	6.62	6.94
0.42	10.78	7.23	7.49	7.81
0.46	11.75	8.10	8.43	8.71
0.50	12.70	8.98	9.37	9.61
0.54	13.66	9.94	10.37	10.55
0.58	14.62	10.93	11.39	11.54
0.62	15.78	12.01	12.48	12.57
0.66	16.93	13.21	13.69	13.69
0.70	18.19	14.49	15.01	14.89
0.75	19.88	16.22	16.79	16.49
0.80	21.63	17.98	18.62	18.18
0.85	23.52	19.82	20.50	19.95
0.90	25.46	21.72	22.42	21.83
0.95	27.54	23.75	24.55	23.92
0.98	29.03	25.40	26.42	25.27
1.00	30.33	27.04	28.17	26.44

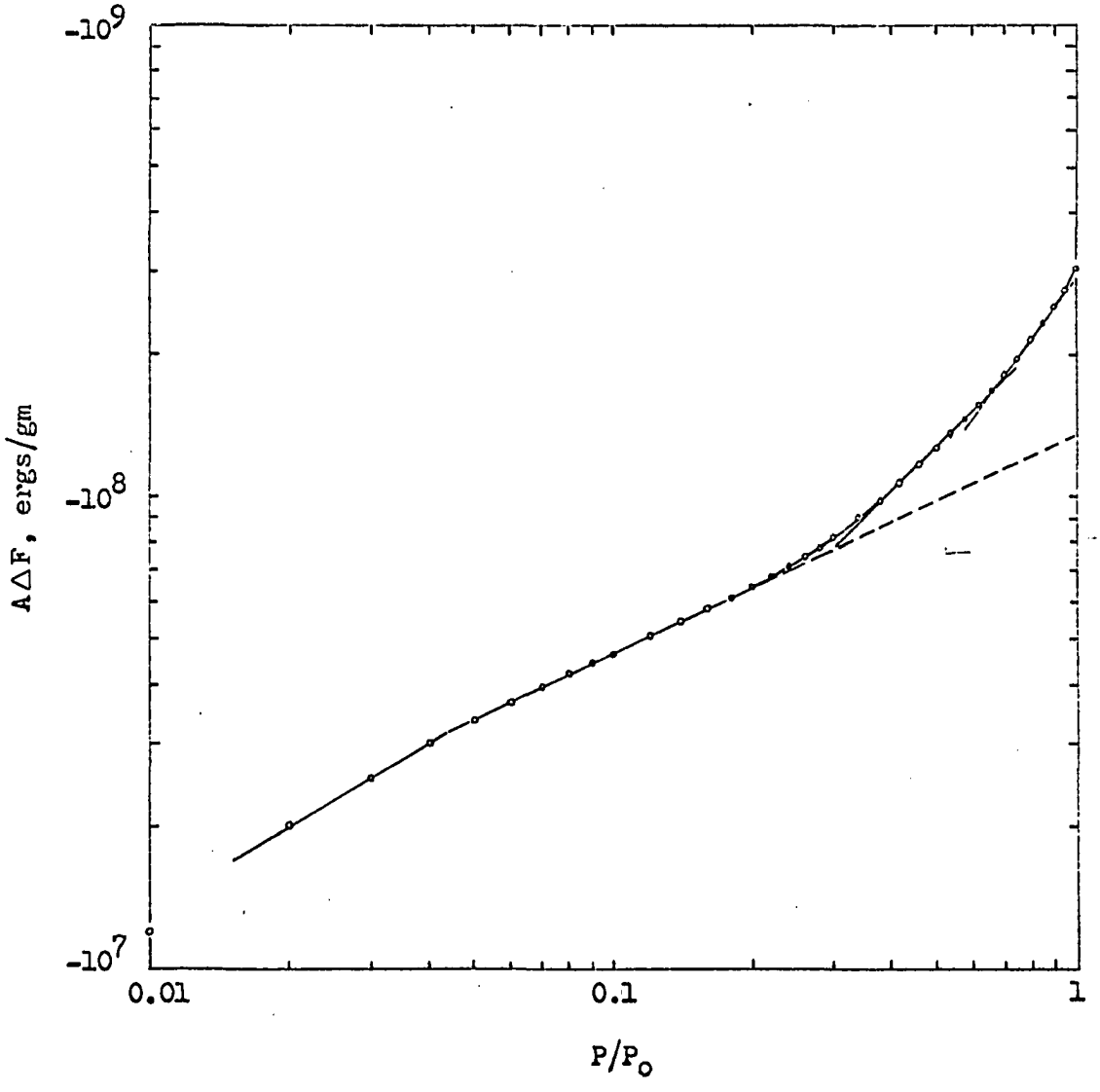

Figure 17. Log-log plot of free energy change versus relative pressure, first adsorption run

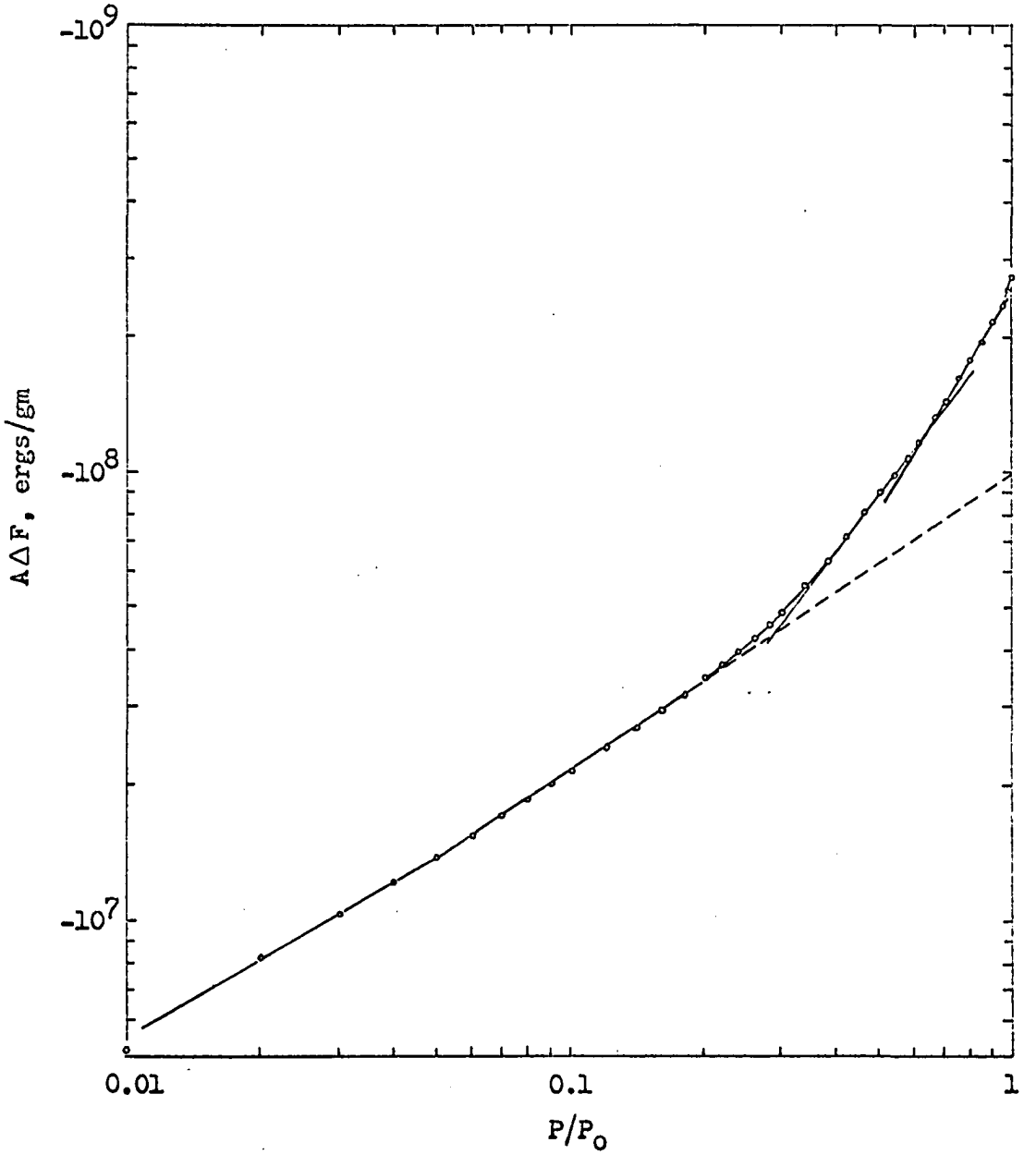

Figure 18. Log-log plot of free energy change versus relative pressure, second adsorption run

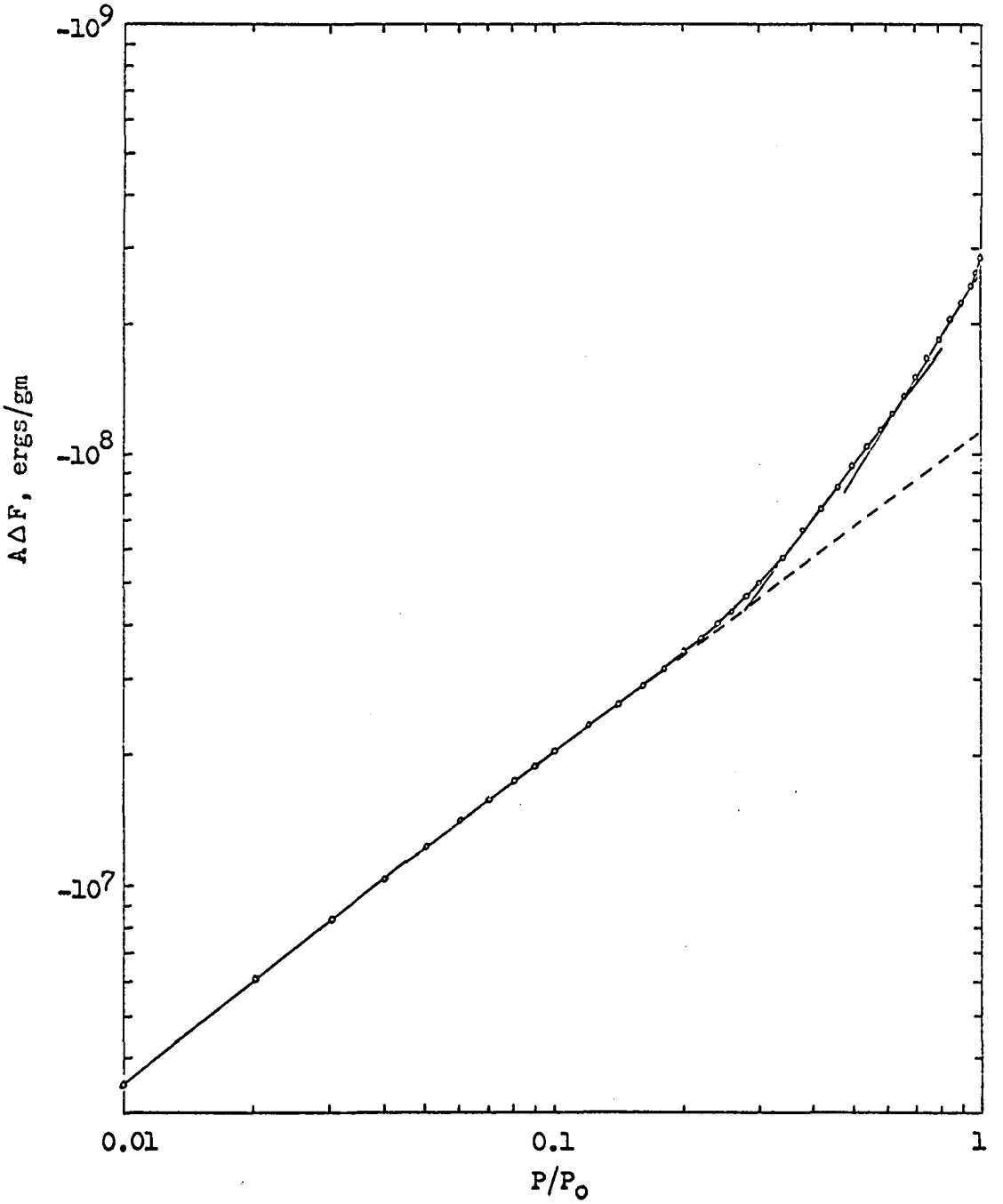

Figure 19. Log-log plot of free energy change versus relative pressure, third adsorption run

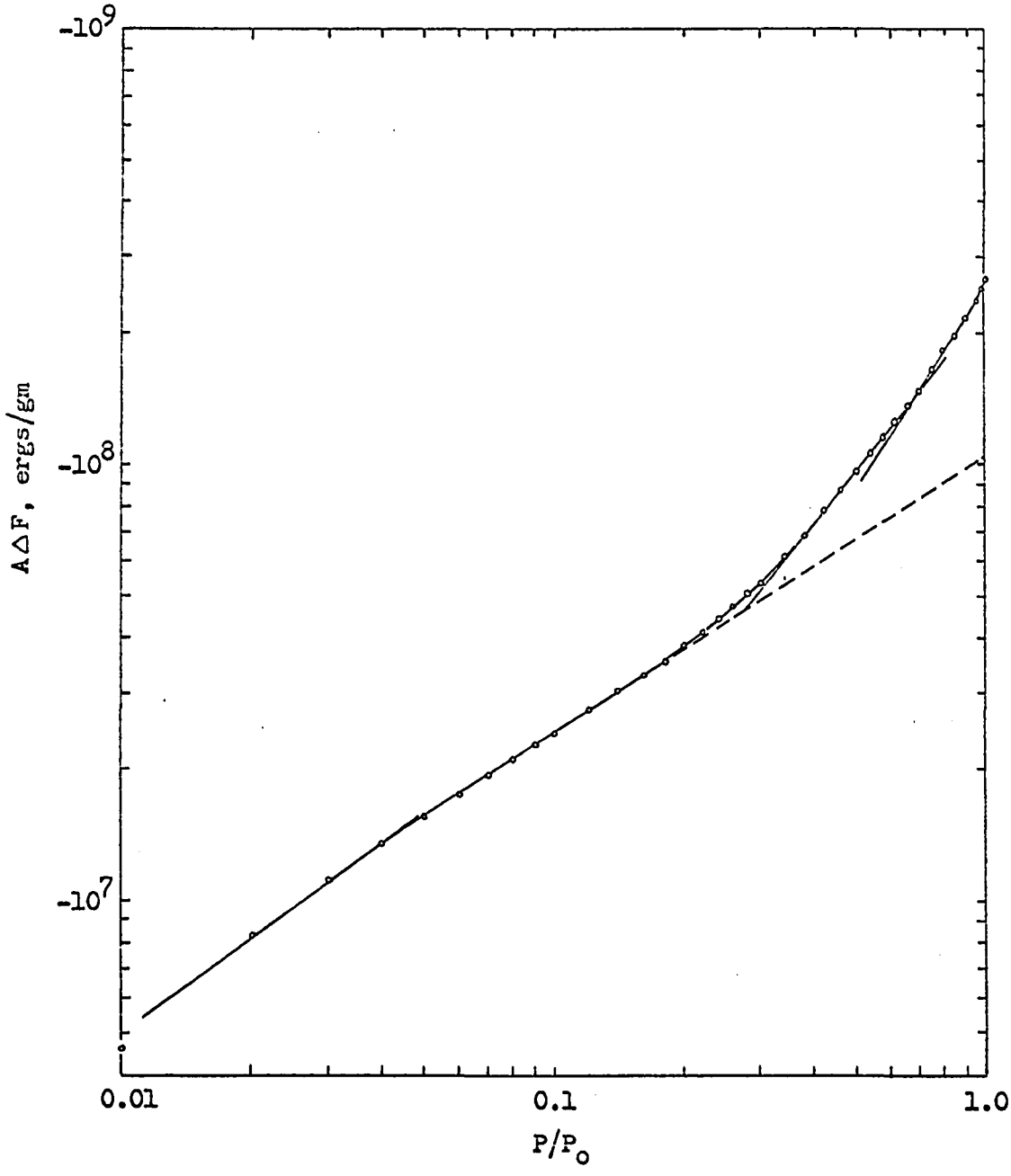

Figure 20. Log-log plot of free energy change versus relative pressure, Demirel's adsorption data

corresponds closely with the beginning of an increase in the basal spacing from 9.8 Å. The break at a p/p_o of about 0.65 corresponds quite closely with the beginning of a second increment of expansion from a basal spacing of about 12.5 Å; the break at a p/p_o of about 0.95 corresponds closely with the beginning of the third increment of expansion from a basal spacing of about 15.5 Å. The last two breaks also correspond very well with observed minima in the plot of line widths versus p/p_o; these minimum line widths indicate that the majority of the clay platelets have the average basal spacing noted. On the basis of these correlations it was concluded that the portion of the log(AΔF) versus log(p/p_o) plot below a p/p_o of 0.16 to 0.18 reflects the energy changes due to adsorption on the external surfaces only; above a p/p_o 0.18 the curve also includes energy changes due to adsorption on the internal surfaces and reflects the energy of interaction between adjacent clay platelets. The slope changes apparently reflect the differences in platelet interaction energies at increasing increments of expansion. If there were no attractive forces between platelets the free energy change due to adsorption on all surfaces of the montmorillonite versus relative humidity would probably follow some relation which would give a smooth log-log plot not displaying the sharp slope changes observed. In the present system, however, expansion must be done against the attractive forces and so the rate of free energy change is reduced. In the p/p_o range

0.18 to 0.65 the first molecular layer of interlayer water is forming and expansion must be accomplished against the platelet interaction energy, ΔV_1, when the platelets are in contact. At a p/p_o of 0.65 a great majority of the platelets are separated by one molecular layer of water (Figure 7); above this relative pressure the second molecular layer is forming and expansion must be done against the interaction energy, ΔV_2, when the layers have a separation of one molecular layer of water, and a change of slope in the plots of Figures 17, 18, 19 and 20 is observed. Similarily, at a p/p_o of 0.95 the interaction energy is ΔV_3 corresponding to a separation of two molecular layers of water and another slope change is observed.

In their study Fu and Bartell (26) attributed the change of slope observed in their $\log(A\Delta F)$ versus $\log(p/p_o)$ plots to capillary condensation in the pores of the adsorbent. In the present system capillary condensation probably occurs in external pore spaces in the higher relative pressure range, but its effect on the energy changes is apparently masked by those caused by adsorption on the internal surfaces. Therefore, the relative pressure at which capillary condensation begins can not be located as it was by Fu and Bartell for adsorption on rigid porous adsorbents. According to Barrer and MacLeod (5) capillary condensation of water between clay particles does not occur until the relative pressure approaches 1.

The relation between the free energy change and separation of clay platelets is shown quite clearly in Figure 21. The values of $A\Delta F$ obtained from Table 15 and Figure 17 for the first adsorption run are plotted against platelet separations h, at the same p/p_o, obtained from Table 2 and Figure 7 (basal spacing plot for the initial adsorption run). $A\Delta F$ data taken from Figures 18, 19 and 20 produce very similar plots. Figure 21 shows sharp breaks in the $A\Delta F$ versus h plot which correspond closely with the slope changes noted in Figure 17. Also, the breaks occur when h values are very nearly integral multiples of 2.8 Å, the thickness of a water molecule. This gives additional evidence that the interlayer water builds up in a laminar fashion. Figure 21 shows that the free energy change due to adsorption on the external surfaces before interlayer expansion begins is about -6×10^7 ergs/gm of sodium montmorillonite. The free energy change for adsorption on all surfaces during formation of the first molecular layer of interlayer water is about -12×10^7 ergs/gm, the change during formation of the second molecular layer is about -9×10^7 ergs/gm, and during formation of the third layer of interlayer water it is about -3×10^7 ergs/gm. As noted, these free energy changes include that due to additional adsorption on the external as well as the internal surfaces of the sodium montmorillonite.

Figure 21. Plot of total free energy change versus interlayer separation, first adsorption run

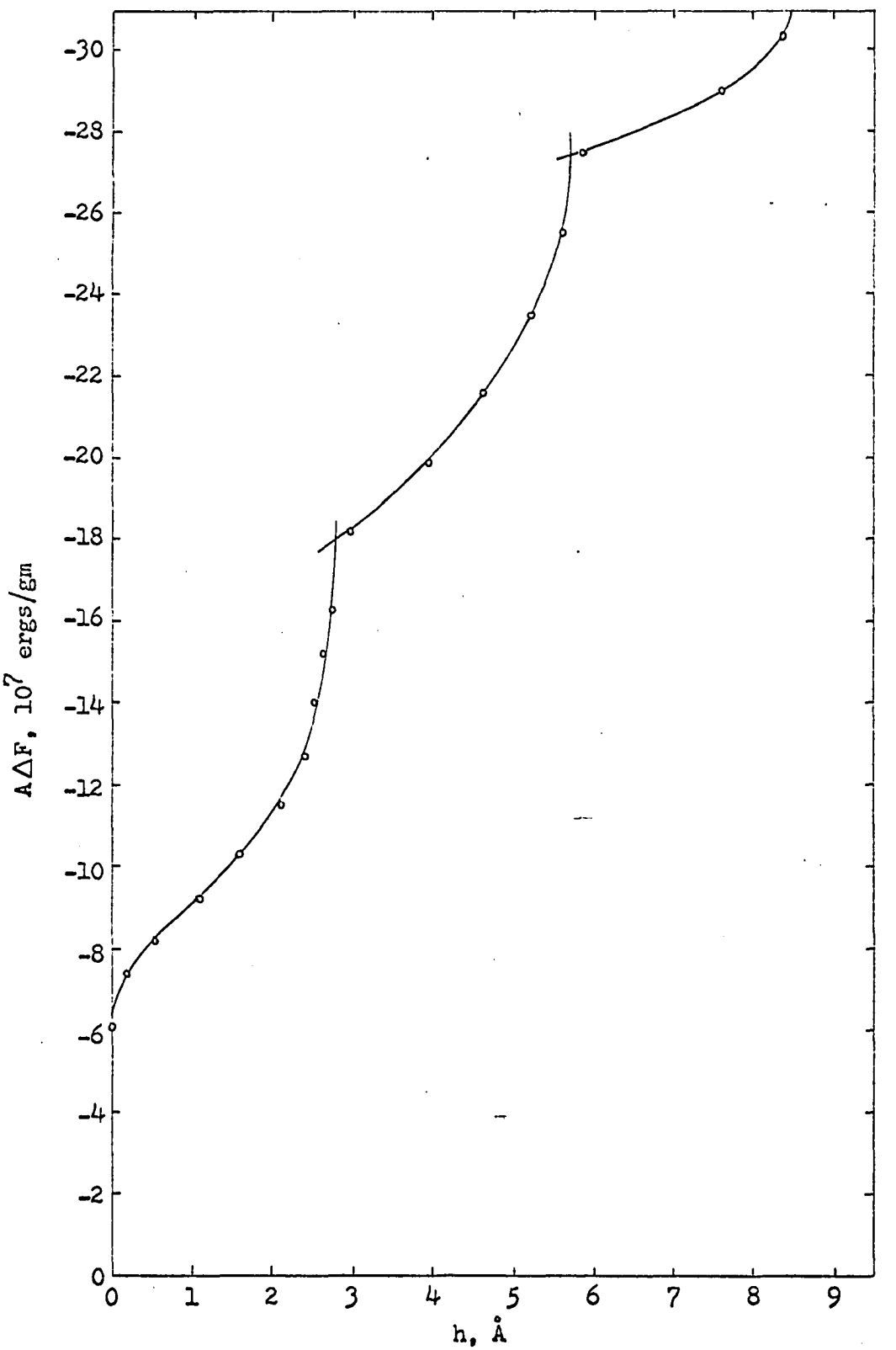
-30
-28
-26
-24
-22
-20
-18
-16
-14
-12
-10
-8
-6
-4
-2
0
0
1
2
3
4
5
6
7
8
9
AΔF, 10^7 ergs/gm
h, Å

Expansion energies

If the free energy changes could be divided into two components, one for adsorption on external surfaces and another for adsorption on internal surfaces, it would be possible to evaluate the expansion energies, i.e. the free energy change due to adsorption on and separation of the internal surfaces.

The free energy change brought about by the adsorption, on a solid surface, of a film at equilibrium with a vapor at some pressure p may be expressed as (1, p. 264; 29, p. 139):

$$\Delta F = \gamma_{sv} - \gamma_{so} \quad \text{ergs/cm}^2 \qquad (9)$$

where γ_{so} is the surface free energy of the solid surface in vacuum and γ_{sv} is that of the solid-vapor interface in equilibrium at pressure p. When the solid-vapor interface is in equilibrium with the saturated vapor the free energy change is:

$$\Delta F = \gamma_{sv^\circ} - \gamma_{so} \quad \text{ergs/cm}^2 \qquad (9a)$$

where γ_{sv° is the surface free energy of the solid-vapor interface at the saturation pressure p_o. According to Jura and Harkins (39) and to Boyd and Livingston (8), when the solid is wetted by the liquid, γ_{sv° is equal to $(\gamma_{sl} + \gamma_{lv})$; γ_{sl} is the solid-liquid interfacial free energy and γ_{lv} is the surface free energy of the liquid in equilibrium with its own vapor. We have, therefore, at saturation:

$$\Delta F = \gamma_{sl} - \gamma_{so} + \gamma_{lv} \quad \text{ergs/cm}^2 \qquad (10)$$

If capillary condensation occurs the γ_{lv} term drops out of Equation 10. For the present system adsorption occurs only on the external surfaces of the clay at low relative pressures. In the relative pressure range 0.05 to 0.18, the linear plot of log(AΔF) versus log(p/p_o) implies that the curve may be expressed by an equation of the type $A\Delta F = \alpha(p/p_o)^{\beta}$. Since only external areas A_e are involved, the free energy change is given by Equation 9:

$$A_e\Delta F = A_e(\gamma_{sv} - \gamma_{so}) \quad \text{ergs/gm} \qquad (9b)$$

If only the external areas were available for adsorption over the entire relative pressure range it is proposed that the relationship $A_e\Delta F = \alpha(p/p_o)^{\beta}$ would continue to be obeyed. Under these circumstances the linear portion of the log(AΔF) versus log(p/p_o) plot between relative pressures of 0.05 to 0.18 would be extended to a p/p_o of 1.0 as shown by the dashed lines on Figures 17 through 20. The free energy change at saturation given by Equation 10 is:

$$A_e\Delta F = A_e(\gamma_{sl} - \gamma_{so} + \gamma_{lv}) \quad \text{ergs/gm} \qquad (10a)$$

If capillary condensation were to occur (still only external surfaces available), a behavior such as that observed by Fu and Bartell (26) would be expected and the free energy change at saturation would be reduced by $A_e\gamma_{lv}$. With the present system this probably occurs very near the saturation pressure and, as noted before, can not be located by the log(AΔF)

versus $\log(p/p_o)$ plot.

On the basis of the above discussion, the free energy changes due to adsorption on external and on internal surfaces were divided, at least to very near saturation, on Figures 17, 18, 19 and 20 by extending the linear portions of the plots corresponding to adsorption on external surfaces only ($A_e\Delta F$) to the saturation pressure. The difference between $A\Delta F$ and $A_e\Delta F$ gives the free energy change $A_i\Delta F = A_i\phi$, where A_i is the internal surface area per gram and ϕ will be designated as the expansion energy per cm^2 of internal surface and given by:

$$\phi = \gamma_{sv} - \gamma_{so} + \Delta V \qquad (11)$$

where ΔV is the free energy change per cm^2 of internal surface due to separation of layers against the force of interaction (56).

Figure 22 presents a plot of $A_i\phi$ obtained from Figure 21 for the first adsorption run versus platelet separation h determined in the same way as for Figure 21. Values of $A_i\phi$ obtained from Figures 18, 19 and 20 produce very similar curves. Figure 22 is quite similar to Figure 21. The value of $A_i\phi$ is about -6.5×10^7 ergs/gm for the first expansion increment and increases to about -14×10^7 ergs/gm and -16.5×10^7 ergs/gm for the second and third expansion increments, respectively. Figure 22 shows that the free energy change due to adsorption of the second molecular layer of interlayer water is as great as or slightly greater than that for

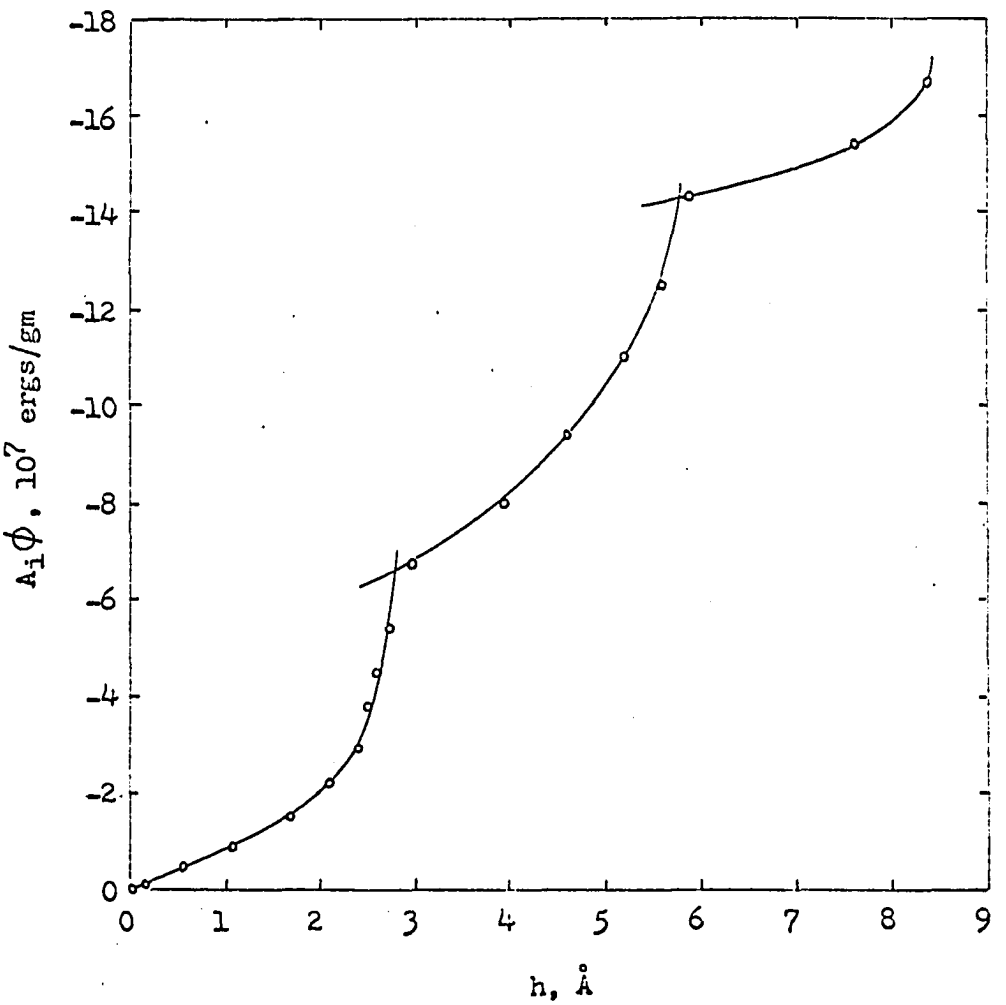

Figure 22. Plot of free energy change due to adsorption on internal surfaces versus interlayer separation, first adsorption run

adsorption of the first molecular layer. The free energy change for formation of the third layer of interlayer water is substantially less than for the other two. The expansion energy ϕ for adsorption of the first layer of interlayer water is the free energy change due to disappearance of a solid surface and the formation of a solid-film interface plus that due to expansion against the interaction energy ΔV_1 when the clay platelets are in contact. The latter term will decrease the magnitude of the free energy change. The second layer of interlayer water must penetrate between the first and the clay surface. No new surfaces are formed nor do any disappear. The free energy change is due to extension of the film thickness and to expansion against the interaction energy ΔV_2 when the clay platelets are separated by one molecular layer of water. Again, the latter term decreases the magnitude of the change. The free energy change due to extension of the film thickness is probably less than that for disappearance of solid surfaces and formation of solid-film interface for the first layer. However, since the platelet separation is greater, ΔV_2 is probably less than ΔV_1 and so the free energy change for formation of the second layer may be nearly the same as that for the first layer. The third layer of water may penetrate between the clay surface and existing interlayer water, but most probably enters between the first and second layer. Again no new surfaces appear of disappear. The free energy change is due to extension of the film thickness and to

expansion against the interaction energy ΔV_3 when the clay platelets are separated by two molecular layers of water. ΔV_3 is probably less than ΔV_2 and ΔV_3 because of increased separation. Since the free energy change on adsorption of the third layer is considerably less than that for the second layer, the change due to penetration between the first and second layers of water must be less than that for penetration between the clay surface and a water layer.

If the internal surface area A_i per gram of sodium montmorillonite were known values for the expansion energy ϕ could be determined. This will be discussed more fully in a later section.

Swelling pressures

Roderick and Demirel (58), in an earlier study, suggested that there was a correlation between free energy data and swelling pressures exerted by montmorillonites. An estimate of the pressure required to prevent separation of clay platelets due to penetration of water between the layers (or the swelling pressure exerted by the clay on uptake of interlayer water) was attempted using the basal spacing and free energy data of the present study.

At constant temperature and assuming all work to be pressure-volume work, we have for free energy:

$$dF = Vdp \qquad (12)$$

where V is the volume of the system and p is the external pressure. For the present system Equation 12 becomes:

$$A_i d\phi = V dp$$

or:

$$d\phi = \frac{V}{A_i} dp = (d_o + h) dp \qquad (13)$$

where ϕ is the expansion energy (change in free energy due to adsorption on and separation of internal surfaces) per cm^2, V is the total volume per gram of sodium montmorillonite, h is the platelet separation, d_o is the initial basal spacing (equal to 9.82 Å) and p is the applied pressure. From Equation 13 we obtain:

$$A_i \int_{\phi=\phi_s}^{\phi=0} \frac{d\phi}{d_o + h} = A_i \int_{p=0}^{p=p^\circ} dp \qquad (14)$$

where ϕ_s is the expansion energy when the clay is in equilibrium with saturated water vapor, p° is the pressure required to prevent <u>any</u> platelet separation and p = 0 is the pressure when the maximum separation is reached. The platelet separation is a function of ϕ as shown in Figure 22. A plot of $1/(d_o + h)$ versus $A_i\phi$ for the first adsorption run is presented in Figure 23 for graphical integration of Equation 14. The pressure required to prevent expansion beyond a certain separation h, when the sodium montmorillonite is in contact

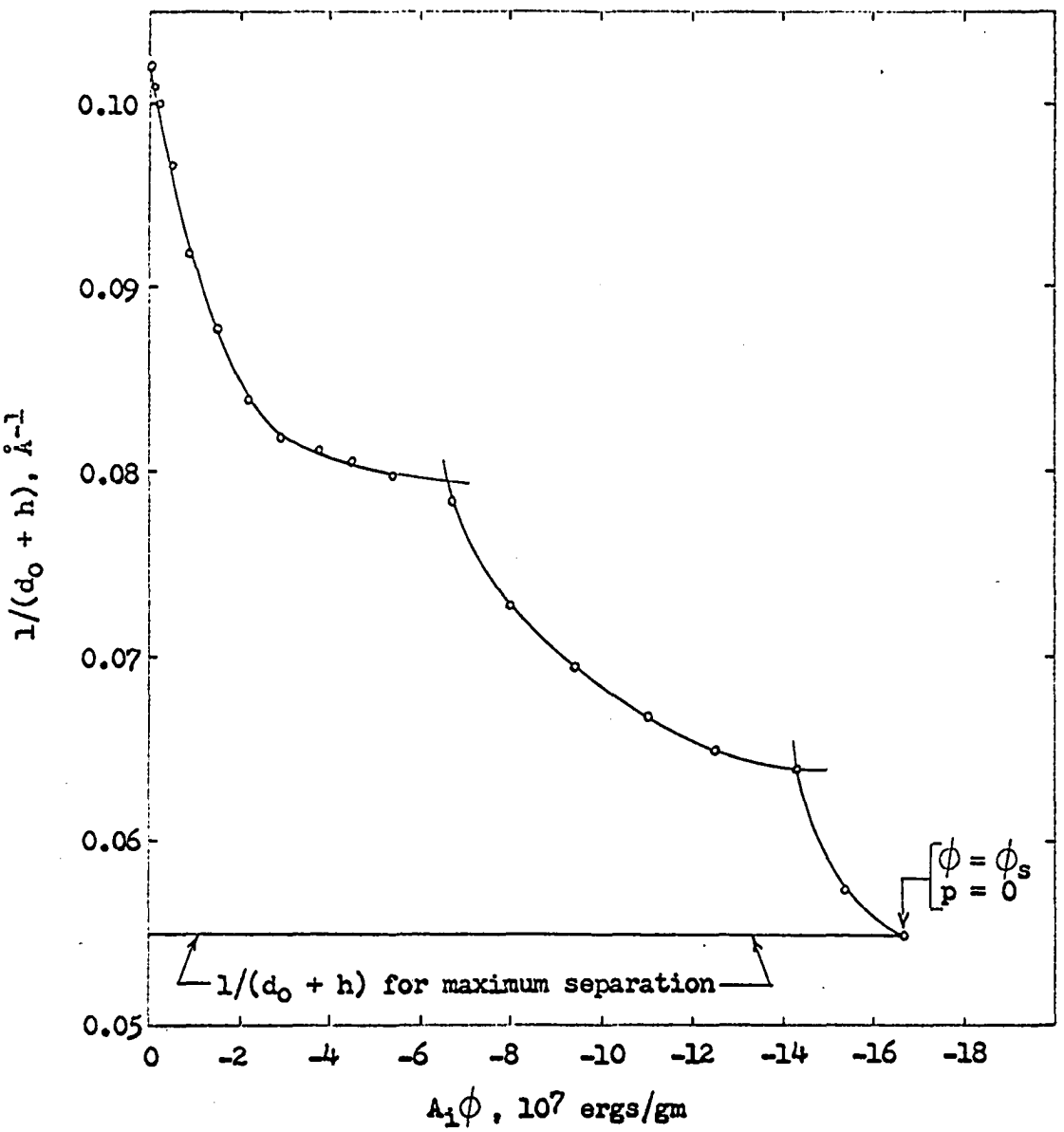

Figure 23. Plot for graphical integration of Equation 14 for the first adsorption run

with saturated water vapor, may be obtained by measuring the area under the curve from $\phi = \phi_s$ to the ϕ corresponding with h. Thus, the pressure required to prevent the uptake of a third layer of interlayer water when the sodium montmorillonite, containing two molecular layers of interlayer water, is in contact with saturated water vapor may be determined from the area under the curve of Figure 23 between the last break point and the end of the curve corresponding to $\phi = \phi_s$ and $p = 0$. Similarily, the pressure required to prevent further expansion beyond that for one molecular layer of interlayer water may be found from the area between the first break and the end of the curve. The pressure p° required to prevent the uptake of any interlayer water may be obtained from the total area under the curve. The areas determined have the dimensions $\frac{ergs}{cm\ gm}$ and must be divided by the internal surface area A_i to give the pressure in dynes/cm^2. Performing the graphical integration, the pressure required to prevent uptake of a third layer of water was found to be about $\frac{7 \times 10^{12}}{A_i}$ dynes/cm^2; that for prevention of uptake beyond the first layer was found to be about $\frac{112 \times 10^{12}}{A_i}$ dynes/cm^2. The pressure p° for prevention of any interlayer adsorption was found to be approximately $\frac{306 \times 10^{12}}{A_i}$ dynes/cm^2.

In order to obtain numerical values for swelling pressures the internal area, A_i, per gram of sodium montmorillonite must be known. Column 2 of Table 13 presents the external

areas, A_e, determined for the first adsorption run by using, in Equation 7, various cross-sectional areas for the water molecule and the parameter q_m from the BET plot of Figure 13. Subtracting A_e from the total surface area of 748 m^2/gm obtained from crystallographic data (see p. 96) gives the internal surface area A_i per gram. The area occupied per molecule for a closest packing arrangement is commonly used in surface area determinations; the corresponding area per water molecule would be 10.8 $Å^2$. The data of the present study gives evidence that the interlayer water builds up in a laminar manner; one such arrangement proposed by Hendricks and Jefferson (31) gives an area of about 11.5 $Å^2$ per water molecule. On the other hand, Demirel (20), from water adsorption data for calcium montmorillonite, obtained a cross-sectional area of about 17.5 $Å^2$ per water molecule. For purposes of comparison, each of the above areas for the water molecule were used to determine the internal surface area, A_i, which was then used to determine the swelling pressures for various interlayer spacings. The results are presented in Table 16. Also presented are values for the expansion energy, ϕ, obtained from the $A_i\phi$ values given on page 112. The differences in the values obtained with the various internal surface areas are probably less than the error due to the approximations of the methods for evaluation of the expansion energies and swelling pressures.

The expansion energy values at saturation may be due

Table 16. Expansion energies and swelling pressures due to adsorption of water vapor on the interlayer surfaces of sodium montmorillonite (from the separation indicated to the maximum separation)

	Area assigned to a water molecule, $Å^2$	Internal surface area, A_i, m^2/gm	Expansion energy, ϕ, $ergs/cm^2$	Swelling pressure, p, $dynes/cm^2$	Swelling pressure, p, $tons/ft^2$
No interlayer water present	10.8	665	--	46.0×10^6	48.3
	11.5	660	--	46.4×10^6	48.7
	17.5	614	--	49.8×10^6	52.3
1 molecular layer of interlayer water	10.8	665	-9.8	16.9×10^6	17.7
	11.5	660	-9.8	17.0×10^6	17.8
	17.5	614	-10.6	18.3×10^6	19.2
2 molecular layers of interlayer water	10.8	665	-21.1	10.5×10^5	1.1
	11.5	660	-21.2	10.6×10^5	1.1
	17.5	614	-22.8	10.6×10^5	1.2
3 molecular layers of interlayer water	10.8	665	-24.8	--	--
	11.5	660	-25.0	--	--
	17.5	614	-26.9	--	--

in part to capillary condensation in external pores. This would tend to make the values given when three molecular layers of water are present somewhat larger than the actual case; the energy change due to adsorption on internal surfaces during formation of the third interlayer of water would probably be somewhat less than indicated by Table 16. The expansion energies given in Table 16 for the adsorption of the first two layers of water are not affected by capillary condensation since it occurs near the saturation pressure.

Since the swelling pressures in Table 16 were obtained by integration of the curve of Figure 23 from the saturation point, any capillary condensation effects would tend to make the listed values somewhat larger than those due only to adsorption on internal surfaces. This may affect the values of swelling pressure when two layers of interlayer water are present to some degree, but would probably be negligible when compared with the large swelling pressures at lower interlayer water contents. Mielenz and King (49) reported swelling pressures from 2 to 11 tons/ft^2 for sodium montmorillonite in consolidometer tests. The present data suggest the pressures they obtained were due to hydration above one layer of interlayer water.

Van Olphen (62) estimated the pressure required to remove a monolayer of water from clay surfaces by dividing the free energy change per cm^2 on desorption by the thickness of one molecular layer of water; apparently he equated the free

energy change to the pressure-volume work. He found the net energy required to remove the last few layers of water from between clay platelets to be from 50 to 100 ergs/cm^2, using the desorption data of Mooney et al. (51,52) for various montmorillonites. The estimated pressure required to remove all water layers would thus be about 2000 tons/ft^2 for an energy change of 50 ergs/cm^2, if calculated by this method. Applying this procedure to the present data, with reservations, the pressure required to prevent uptake of water would be $\Delta F/2.8 \times 10^{-8}$, where ΔF is -40.6 ergs/cm^2 for the first adsorption run. This would give a pressure of about 1450 tons/ft^2 required to prevent expansion. This procedure does not attempt to divide the free energy changes due to adsorption on external and internal surfaces; during adsorption from the vapor phase most of the volume change is probably due to separation of the internal surfaces, very little being caused by adsorption on external surfaces.

It should be emphasized that the swelling pressures tabulated in Table 16 are those exerted when the sodium montmorillonite is in contact with saturated water vapor; the maximum observed interlayer separation is in equilibrium with the saturated vapor. If the sodium montmorillonite were in contact with liquid water further expansion would occur and comparatively smaller swelling pressures may develop. In this region, for separations beyond that for three or four molecular layers of water, the surface hydration energies are

no longer important and the smaller electrical double-layer forces become the major repulsive force between platelets (62). The further expansion exerting comparatively low additional pressure may be explained by attributing it to a low energy barrier (20).

CONCLUSIONS

The sorption isotherm data and X-ray diffraction data for water vapor adsorption and desorption by sodium montmorillonite, and data from the literature, indicate that:

1. The change in average basal spacings of sodium montmorillonite takes place in a continuous but non-uniform manner with changes in relative pressure; continuity is due to the simultaneous existence of varying numbers of molecular layers of interlayer water. Expansion occurs in three increments; basal spacing and line width data show average spacings correspond with an integral number of molecular layers of interlayer water just prior to each increment of expansion.

2. The relationship between relative humidity and the basal spacing of sodium montmorillonite is dependent on: a) the source and method of preparation of the sample, b) the initial conditions of the sample at the start of the test, and c) whether data is collected during adsorption or desorption.

3. Basal spacing, line width and free energy change data give evidence that interlayer water builds up in a laminar manner.

4. Adsorption isotherms are more closely reproduced on successive adsorption-desorption runs than are desorption isotherms.

5. The hysteresis displayed by the sorption isotherms is due in part to the formation of a thixotropic structure at

high relative pressures, and in part to attractive interaction forces between sodium montmorillonite platelets.

6. X-ray diffraction data and BET plots indicate that the BET parameter q_m obtained reflects adsorption only on the external surfaces of the sodium montmorillonite; apparently sodium montmorillonite prepared from Wyoming bentonite is unique in this respect. The total surface area can not be determined by the BET method for water vapor adsorption.

7. The heats of adsorption less the heat of liquefaction of water for the first molecular layer of water adsorbed on the external surface, as determined from the BET parameter C, is about 3 Kcal/mole. This is in good agreement with values found by others, and with values calculated from calorimetric heat of immersion data from the literature (63).

8. The free energy of wetting of sodium montmorillonite, defined as the free energy of immersion less the free energy change in particle interaction, was determined by use of Bangham's free energy equation to be -40.55, -36.15 and -37.30 ergs/cm^2 for the three adsorption runs; this is in good agreement with the value of -34.76 ± 1.91 ergs/cm^2 obtained by Demirel (20).

9. The relationship between free energy changes and relative pressure and the X-ray diffraction data for the adsorption of water vapor by sodium montmorillonite allows separation of the free energy change into two components, one due to adsorption on the external surfaces and one due to

adsorption on the external surfaces and one due to adsorption on and separation of the internal surfaces.

10. Free energy data and X-ray diffraction data show that the expansion energy (free energy change due to adsorption on and separation of internal surfaces) during formation of the second layer of interlayer water is approximately the same as that for formation of the first layer; the change during formation of the third layer is substantially less than those for the other two.

11. Free energy data and X-ray diffraction data permit the estimation of swelling pressures exerted by sodium montmorillonite due to the uptake of interlayer water when the material is in contact with saturated vapor. The swelling pressure exerted when the platelet separation is zero is about 50 tons/ft^2. The pressure exerted when one molecular layer of water separates clay platelets is about 18 tons/ft^2; that when two molecular layers of water separate platelets is about 1.1 tons/ft^2.

LITERATURE CITED

1. Adamson, A. W. Physical chemistry of surfaces. New York, N.Y., Interscience Publishers, Inc. 1960.

2. Armbuster, M. H. A. and Austin, J. B. The adsorption of gases on smooth surfaces of steel. American Chemical Society Journal 66: 159-171. 1944.

3. Bangham, D. H. The Gibbs adsorption equation and adsorption on solids. Faraday Society Transactions 33: 805-811. 1937.

4. Bangham, D. H. and Razouk, R. I. Adsorption and wettability of solid surfaces. Faraday Society Transactions 33: 1459-1463. 1937.

5. Barrer, R. M. and MacLeod, D. M. Intercalation and sorption by montmorillonite. Faraday Society Transactions 50: 980-989. 1954.

6. Barshad, I. The nature of lattice expansion and its relation to hydration in montmorillonite and vermiculite. American Mineralogist 34: 675-684. 1949.

7. Bartell, F. E. and Dobay, D. G. The adsorption of aliphatic amine vapors by silica gel. American Chemical Society Journal 72: 4388-4393. 1950.

8. Boyd, G. E. and Livingston, H. K. Adsorption and energy changes at crystalline solid surfaces. American Chemical Society Journal 64: 2383-2388. 1942.

9. Bradley, W. F., Grim, R. E. and Clark, G. L. A study of the behavior of montmorillonite upon wetting. Zeitschrift für Kristallographie 97: 216-222. 1937.

10. Brindley, G. W. Experimental methods. In Brown, G., ed. The x-ray identification and crystal structures of clay minerals. pp. 1-50. London, Mineralogical Society. 1961.

11. Brindley, G. W. Quantitative analysis of clay mixtures. In Brown, G., ed. The x-ray identification and crystal structures of clay minerals. pp. 489-516. London, Mineralogical Society. 1961.

12. Brindley, G. W. X-ray diffraction by layer lattices with random layer displacements. In Brown, G., ed. The X-ray identification and crystal structures of clay minerals. pp. 446-466. London, Mineralogical Society. 1961.

13. Brunauer, S. The adsorption of gases and vapors. Physical adsorption. Princeton, N.J., Princeton University Press. 1943.

14. Brunauer, S. Solid surfaces and solid-gas interface. Advances in Chemistry Series 33: 5-17. 1961.

15. Brunauer, S., Deming, L. S., Deming, W. E. and Teller, E. On a theory of the van der Waals adsorption of gases. American Chemical Society Journal 62: 1723-1732. 1940.

16. Brunauer, S., Emmett, P. H. and Teller, E. Adsorption of gases in multimolecular layers. American Chemical Society Journal 60: 309-319. 1938.

17. Clampitt, B. H. and German, D. E. Heat of vaporization of molecules at liquid-vapor interfaces. Journal of Physical Chemistry 62: 438-440. 1958.

18. Craig, R. G., Van Voorhis, J. J. and Bartell, F. E. Free energy of immersion of compressed powders with different liquids. I. Graphite powders. Journal of Physical Chemistry 60: 1225-1230. 1956.

19. Deitz, V. R. Gas adsorption, the extreme limits of surface coverage. Industrial and Engineering Chemistry 57, No. 5: 49-66. 1965.

20. Demirel, T. Adsorption of water vapor by sodium and calcium montmorillonites. Unpublished Ph.D. thesis. Ames, Iowa, Library, Iowa State University of Science and Technology. 1962.

21. Dobay, D. G., Fu, Y. and Bartell, F. E. Energetics of the adsorption of aliphatic amines by silica gel. American Chemical Society Journal 73: 308-314. 1951.

22. Emmett, P. H., Brunauer, S. and Love, K. S. The measurement of surface area of soils and soil colloids by the use of low temperature van der Waals adsorption isotherms. Soil Science 45: 57-65. 1938.

23. Forslind, E. Crystal structure and water adsorption of clay minerals. Swedish Cement and Concrete Research Institute Bulletin 11: 1-20. 1948.

24. Forslind, E. Some remarks on the interaction between the exchangeable ions and the adsorbed water layers in montmorillonite. 4th International Congress of Soil Science, Transactions 1: 110-113. 1950.

25. Foster, A. G. The sorption of condensible vapors by porous solids. I. The applicability of the capillary theory. Faraday Society Transactions 28: 645-657. 1932.

26. Fu, Y. and Bartell, F. E. Surface area of porous adsorbents. Journal of Physical and Colloid Chemistry 55: 662-675. 1951.

27. Gillery, F. H. Adsorption-desorption characteristics of synthetic montmorillonoids in humid atmospheres. American Mineralogist 44: 806-818. 1959.

28. Goates, J. R. and Hatch, C. V. Standard adsorption potentials of water vapor on soil colloids. Soil Science 75: 275-278. 1953.

29. Gregg, S. J. The surface chemistry of solids. 2nd ed. New York, N.Y., Reinhold Publishing Corporation. 1961.

30. Grim, R. E. Clay mineralogy. New York, N.Y., McGraw-Hill Book Company, Inc. 1953.

31. Hendricks, S. B. and Jefferson, M. E. Structure of kaolin and talc-pyrophyllite hydrates and their bearing on water sorption of clays. American Mineralogist 23: 863-875. 1938.

32. Hendricks, S. B., Nelson, R. A. and Alexander, L. T. Hydration mechanism of the clay mineral montmorillonite saturated with various cations. American Chemical Society Journal 62: 1457-1464. 1940.

33. Hirst, W. The mechanical interaction between mobile insoluble adsorbed films, capillary condensed liquid and fine-structured solids. Faraday Society Discussions 3: 22-28. 1948.

34. Hodgman, C. D., Weast, R. C., Shankland, R. S. and Selby, S. M., eds. Handbook of chemistry and physics. 44th ed. Cleveland, Ohio, The Chemical Rubber Publishing Co. 1963.

35. Inness, W. B. and Rowley, H. H. Relationship between the adsorption isotherm and the spreading forces. Journal of Physical Chemistry 45: 158-165. 1941.

36. Johansen, R. T. and Dunning, H. N. Water-vapor adsorption on clays. National Conference on Clays and Clay Minerals, Proceedings 6: 249-258. 1959.

37. Johns, W. D., Grim, R. E. and Bradley, W. F. Quantitative estimations of clay minerals by diffraction methods. Journal of Sedimentary Petrology 24: 242-251. 1954.

38. Jonas, E. C. and Roberson, H. E. Particle size as a factor influencing expansion of the three-layer clay minerals. American Mineralogist 45: 828-838. 1960.

39. Jura, G. and Harkins, W. E. Determination of the decrease of free surface energy of a solid by an adsorbed film. American Chemical Society Journal 66: 1356-1362. 1944.

40. Klug, H. P. and Alexander, L. E. X-ray diffraction procedures for polycrystalline and amorphous materials. New York, N.Y., John Wiley and Sons, Inc. 1954.

41. Livingston, H. K. The cross-sectional areas of molecules adsorbed on solid surfaces. Journal of Colloid Science 4: 447-457. 1949.

42. Macey, H. H. Clay-water relationships and the internal mechanism of drying. Ceramic Society Transactions 41: 73-121. 1942.

43. MacEwan, D. M. C. Montmorillonite minerals. In Brown, G., ed. The x-ray identification and crystal structures of clay minerals. pp. 143-207. London, Mineralogical Society. 1961.

44. MacEwan, D. M. C., Amil, A. R. and Brown, G. Interstratified clay minerals. In Brown, G., ed. The x-ray identification and crystal structures of clay minerals. pp. 393-445. London, Mineralogical Society. 1961.

45. McBain, J. W. An explanation of hysteresis in the hydration and dehydration of gels. American Chemical Society Journal 57: 699-700. 1935.

46. McBain, J. W. and Bakr, A. M. A new sorption balance. American Chemical Society Journal 48: 690-695. 1926.

47. Mering, J. On the hydration of montmorillonite. Faraday Society Transactions 42B: 205-219. 1946.

48. Messina, M. L. Expansion of fractional montmorillonites under various relative humidities. Clays and Clay Minerals 19: 617-632. 1964.

49. Mielenz, R. C. and King, M. E. Physical-chemical properties and engineering performance of clays. State of California Department of Natural Resources, Division of Mines Bulletin 169: 196-254. 1955.

50. Milne, I. H. and Warshaw, C. M. Methods of preparation and control of clay mineral specimens in x-ray diffraction analysis. National Conference on Clays and Clay Minerals, Proceedings 4: 22-30. 1956.

51. Mooney, R. W., Keenan, A. G. and Wood, L. A. Adsorption of water vapor by montmorillonite. I. Heat of desorption and application of BET theory. American Chemical Society Journal 74: 1367-1371. 1952.

52. Mooney, R. W., Keenan, A. G. and Wood, L. A. Adsorption of water vapor by montmorillonite. II. Effect of exchangeable ions and lattice swelling as measured by x-ray diffraction. American Chemical Society Journal 74: 1371-1374. 1952.

53. Nagelschmidt, G. On the lattice shrinkage and structure of montmorillonite. Zeitschrift für Kristallographie 93: 481-487. 1936.

54. National Research Council of the United States of America. International critical tables. Vol. 1. New York, N.Y., McGraw-Hill Book Company, Inc. 1926.

55. Orchiston, H. D. Adsorption of water vapor. III. Homoionic montmorillonites at 25° C. Soil Science 79: 71-78. 1955.

56. Overbeek, J. T. G. The interaction between colloidal particles. In Kruyt, H. R. Colloid science. Vol. 1. pp. 245-277. New York, N.Y., Elsevier Publishing Company. 1952.

57. Pauling, L. The nature of the chemical bond. Ithaca, N.Y., Cornell University Press. 1960.

58. Roderick, G. L. and Demirel, T. Expansion of montmorillonite due to adsorption of water vapor. Iowa Academy of Science Proceedings 70: 280-289. 1963.

59. Takizawa, M. Mechanism of water vapor adsorption on bentonite. Tokyo Institute of Physical and Chemical Research Scientific Papers 54: 313-322. 1960.

60. Topping, J. Errors of observation and their treatment. London, The Institute of Physics. 1957.

61. van Olphen, H. Interlayer forces in bentonite. National Academy of Sciences - National Research Council Publication 327: 418-438. 1954.

62. van Olphen, H. An introduction to clay colloid chemistry. New York, N.Y., Interscience Publishers. 1963.

63. Zettlemoyer, A. C., Young, G. J. and Chessick, J. J. Studies of the surface chemistry of silicate minerals. Journal of Physical Chemistry 59: 962-966. 1955.

ACKNOWLEDGMENTS

This investigation was conducted as part of the research being done under Project 505-S of the Engineering Experiment Station, Iowa State University of Science and Technology. The project is sponsored by the Iowa Highway Research Board under Project HR 97, and is supported by funds supplied by the Iowa State Highway Commission and the U.S. Bureau of Public Roads.

I wish to express my sincere appreciation to Dr. T. Demirel, Associate Professor of Civil Engineering, for guidance and assistance given throughout the investigation. I also wish to thank Larry R. Moore for his help in designing and constructing equipment used in the study.